Superparamagnetic iron oxide nanoparticles: from preparations to in vivo MRI applications†

Ruirui Qiao, Chunhui Yang and Mingyuan Gao*

Received 4th February 2009, Accepted 9th April 2009
First published as an Advance Article on the web 19th May 2009
DOI: 10.1039/b902394a

Superparamagnetic iron oxide nanoparticles have received great attention due to their applications as contrast agents for magnetic resonance imaging (MRI). This feature article briefly introduces the concepts of MRI and MRI contrast agents, and then mainly discusses the synthesis, surface modification, surface functionalization, colloidal stability and biocompatibility of iron oxide particles, followed by their MRI applications.

1. Introduction

Nanoscience and nanotechnology have gained significant momentum in recent years to interplay with biology and medical science, leading to the emergence of a new interdisciplinary field called "nanomedicine".[1] Nanomedicine can be defined as a new technology for medical diagnosis and treatment based on the special physical effects of nano-objects. Nanotechnology-based devices and nanomaterials have been demonstrated to be greatly useful for improving the efficiency and efficacy of bioassays and medical diagnosis. Among different types of nanomaterials, magnetic iron oxide nanoparticles as magnetic resonance imaging (MRI) contrast agents have set the most successful example for medical applications of inorganic nanoparticles.[2,3] Up to now, several magnetic iron oxide-based contrast agents have been approved with a few others being at different stages of clinical trials. The successful use of magnetic iron oxide particles in monitoring stem cell trafficking and the use of bio-vectorized particles for target-specific imaging make the iron oxide-based contrast agents a new type of MRI molecular probe for visualizing biological events down to cell and even molecular level, consequently leading the iron oxide-based "MR molecular imaging" to a booming area.

Over the past three years, more than 10 review articles have been published on various aspects of magnetic iron oxide particles ranging from chemical synthesis,[4–7] magnetism engineering,[8] surface engineering[9] to in vivo applications.[2,3,10,11] As a matter of fact, most clinical investigations carried out so far are based on the FDA-approved iron oxide-based contrast agents which are produced by a classic hydrolytic synthetic route. However, the hydrolytic synthetic routes, which will be introduced in more detail later in this feature article, have several intrinsic drawbacks, typically resulting in broad particle size distributions, complicated surface compositions, and relatively low crystallinity degrees for the resultant iron oxide particles. In this context, thanks have to be given to a novel non-hydrolytic synthetic route, *i.e.*, a thermal decomposition method firstly introduced by Alivisatos[12] and latterly developed by Hyeon,[13–15] Sun,[16,17] Peng,[18] Cheon,[19] and Gao.[20–25] This method offers great advantages over the hydrolytic synthetic route regarding the mono-dispersity as well as the magnetic susceptibility of the resultant particles (due to higher crystallinity degree and purer

Institute of Chemistry, CAS, Zhong Guan Cun, Bei Yi Jie 2, Beijing, 100190, China. E-mail: gaomy@iccas.ac.cn; Fax: +86 10 82613214; Tel: +86 10 82613214

† This paper is part of a *Journal of Materials Chemistry* theme issue on inorganic nanoparticles for biological sensing, imaging, and therapeutics. Guest editor: Jinwoo Cheon.

Ruirui Qiao received her Masters Degree in Medicinal Chemistry in 2007 from the School of Pharmaceutical Science, Peking University. Since then, she has been working with Prof. Mingyuan Gao in the Institute of Chemistry, the Chinese Academy of Sciences, as a research assistant. Her major research interests are the development and application of iron oxide particle-based molecular imaging probes for cancer detection.

Dr Chunhui Yang received her PhD degree in Medicinal Chemistry from the School of Pharmaceutical Sciences, Peking University in 2008. Since then, she has been working in the group of Prof. Mingyuan Gao in the Institute of Chemistry, the Chinese Academy of Sciences. Her research focuses on the synthesis of inorganic nanocrystals and organic/inorganic nanocomposites, as well as their applications in environmental analysis.

phases) in addition to a facile scaling-up possibility,[15] thus offering great opportunities for fabricating high performance contrast agents. Nevertheless, the direct products of the thermal decomposition method are typically not water-soluble, and because of this drawback further surface chemical modifications are needed to enable them to become useful as high performance magnetic contrast agents. The aim of this feature article is to summarize the state of the art of the advanced synthetic chemistry and set a bridge between synthetic chemistry, surface chemistry and the biomedical applications of magnetic iron oxide particles in MR molecular imaging.

2. MRI and contrast agents

2.1 A brief introduction of the MRI technique

Imaging of human internal organs with high spatial resolution is very important for medical diagnosis, treatment and follow-up. In this respect, magnetic resonance imaging (MRI) marks a very important breakthrough as it offers the ability to achieve extraordinarily high temporal and spatial resolution in addition to its non-invasive feature in comparison with X-ray-based imaging techniques. MRI was invented in the early 1970s.[26] The first commercial setup capable of human scanning appeared about 10 years later.[27] Now it has become one of the most important and powerful clinical diagnostic tools.

The fundamental working principle of MRI is based on computer-assisted imaging of relaxation signals of proton spins within the human body excited by radiofrequency waves in a strong magnetic field. Most commonly water protons are imaged. If the water protons are existing in identical magnetic environments, they will resonate at the same frequency. Then, the nuclear magnetic resonance signal is simply proportional to the volume of water. The key innovation for MRI is to impose spatial variations on the magnetic field to distinguish spins by their locations. A magnetic gradient causes water protons at different locations to oscillate at distinct frequencies, consequently giving rise to a map of the spatial distribution of nuclear spins. More fundamental physical principles and technical details on MRI can be found in numerous publications.[26,28–31]

Dr Mingyuan Gao is currently a full Professor in the Institute of Chemistry, the Chinese Academy of Sciences. His main research interests include: synthesis of nanocrystals with novel properties and unusual shapes and structures; synthesis of organic/inorganic hybrid materials; biological, biomedical and environmental applications of functional nanomaterials. He took his current position upon a "Hundred-talent Program" from CAS. He received the "National Science Fund for Distinguished Young Scholars" from NSFC in 2002. He was an AvH fellow between 1996 and 1998. More details can be found at http://www.gaomingyuan.com.

The relaxation of proton spins to their equilibrium states *via* two processes, namely longitudinal relaxation, characterization by a relaxation time T1, and transverse relaxation, characterized by a relaxation time T2. Typically in soft tissues T1 is around 1 second while T2 is a few tens of milliseconds, but these values vary widely among different tissues in addition to their dependence on external magnetic fields, giving MRI its tremendous soft tissue contrast.[27]

2.2 MRI contrast agents

In spite of the excellent image quality of non-enhanced MRI, various types of contrast agents have been developed to further enhance the contrast between diseased and healthy tissues. The MRI contrast agents principally work by shortening the T1 or T2 relaxation times of protons located nearby. Reduction of the T1 relaxation time results in a hypersignal and consequently gives rise to a positive contrast, while reduced T2 relaxation time reduces both T2 and T2* (describing the decay of transverse magnetization taking into account the inhomogeneity of local static magnetic fields) signals leading to a negative contrast. Typically, elements with unpaired electron spins such as gadolinium, manganese, and iron, can effectively reduce the T1 relaxation time. Therefore various types of small molecular weight metal-organic complexes containing the aforementioned active metal elements have been developed and used as positive contrast agents. The most successful type which has widely been investigated consists of gadolinium-based small molecular complexes, *e.g.*, Ga-DTPA (DTPA = diethylenetriaminepentaacetic acid).[32,33] In contrast, superparamagnetic nanoparticles such as maghemite (γ-Fe_2O_3) and magnetite (Fe_3O_4) nanocrystals can produce predominantly spin–spin relaxation effects due to the induced local field inhomogeneities,[34] consequently resulting in shorter T1 and T2 relaxation times. Up to now, magnetic iron oxide nanoparticles are predominately used as T2 contrast agents, producing negative enhancement effects on T2- and T2*-weighted images. Table 1 presents iron oxide contrast agents which are commercialized or at different clinical stages.

2.3 Special effects of iron oxide-based contrast agents

Different from paramagnetic small molecular weight T1 contrast agents, the magnetic iron oxide-based contrast agents possess tremendous effects in disease detection due to their much bigger size which gives rise to remarkable interactions with blood proteins, mononuclear phagocytic cells, macrophage in tissues, cancer cells, biological barriers, *etc*. In fact, all these interactions are not only related to the particle size but also strongly determined by particle surface physiochemical properties, leading to different fates for various types of iron oxide contrast agents, by which different diagnostic methodologies are being developed. Therefore, the magnetic susceptibility, hydrodynamic size, size distribution, and surface physiochemical properties of the particle contrast agents are the most important parameters with respect to their biomedical applications.

For in vivo applications, the hydrodynamic size of iron oxide particles becomes more important than the size in the dry state due to the fact that the human body is a water-rich system. Therefore, the iron oxide-based contrast agents are generally

Table 1 List of iron oxide contrast agents which are commercialized or at different clinical stages[a]

Compound	Classification	Size	Coating agent	$T_{1/2}$	Indication	Development	Tradename
Ferristene (OMP)	SPIO	3500 nm (composed of crystals below 50 nm)	Sulfonated styrene-divinylbenzene copolymer	Oral	Gastrointestinal	Sale	Abdoscan® (GE-Healthcare)
Ferumoxsil (AMI-121)	SPIO	300 nm (composed of 10 nm crystals)	Siloxane	Oral	Gastrointestinal	Sale	GastroMARK® (Advanced Magnetics); Lumirem® (Guerbet)
Ferrixan (Ferucarbotran, SHU 555A)	SPIO	60 nm	Dextran	2.4–3.6 h	Liver	Sale	Resovist® (Schering); Cliavist™ (Medicadoc)
Ferumoxide (AMI-25, SHU 555A)	SPIO	120–180 nm; 80–150 nm	Dextran	6 min	Liver	Sale	Feridex® (Advanced Magnetics); Endorem™ (Guerbet)
(SHU 555 C)	USPIO	≤20 nm	Dextran	6 h	Angiography	Phase 1	Supravist™ (Schering)
Ferumoxtran-10 (AMI-227, BMS-180549)	USPIO	20–40 nm	Dextran	24–36 h	Lymph node, liver, angiography	Phase 3	Combidex® (Advanced Magnetics); Sinerem® (Guerbet)
Feruglose (PEG-feron, NC100150)	USPIO	Core size 5–7 nm; total size 20 nm	Carbohydrate-polyethylene glycol coating (PEGylated starch)	6 h	Lymph node, liver, perfusion, angiography	Preclinical	Clariscan™ (GE-Healthcare)
(VSOP-C184)	USPIO	7 nm	Citrate	0.6–1.3 h	Angiography	Preclinical	

[a] $T_{1/2}$: blood half-time.

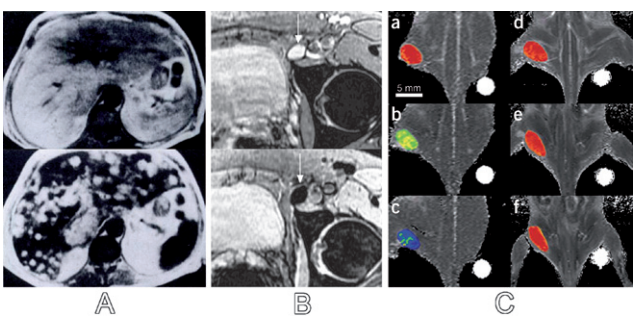

Fig. 1 A) T2-weighted liver images of a patient with metastatic renal cell carcinoma prior to administration (upper) and 15 min post-administration of AMI-25 (lower); B) T2-weighted MR images of lymph node acquired from a patient with prostate cancer prior to administration (upper) and 24 h after administration of Combidex (lower); C) T2-weighted MR images of a mouse implanted with the cancer cell line NIH3T6.7 acquired at different time points after injection of $MnFe_2O_4$-herceptin conjugates or CLIO-herceptin conjugates (pre-injection image (a,d); and 1 h (b, e) or 2 h (c, f) after injection). In a–c, gradual color changes at the tumor site, from red to blue, indicate progressive targeting by $MnFe_2O_4$-herceptin conjugates. In contrast, almost no change is seen in the mouse treated with CLIO-herceptin conjugates (d–f). (Images A, B, and C are reprinted from ref. 140, 36, and 37, respectively, with permissions.)

classified according to their hydrodynamic size. Typically, particles with hydrodynamic size larger than 40 nm are called SPIO (small particle of iron oxide) contrast agents, while those with hydrodynamic size smaller than 40 nm are called USPIO (ultra-small particle of iron oxide) contrast agents.[3] Nevertheless, there is hardly a sharp border between USPIO and SPIO.

In general, the SPIOs are quickly taken up by the reticuloendothelial system (RES) and eventually accumulate in the liver or spleen as the normal function of these organs is to purify the blood of foreign particles. Consequently, SPIOs have been widely developed for detecting lesions and even tumors in the liver, as shown in Fig. 1.

Different from SPIOs, the USPIO type of contrast agent, partly due to their much smaller size, do not accumulate in the RES system as fast as their larger counterparts, therefore they present longer blood circulating times. It is observed that after USPIOs smaller than 10 nm are intravenously injected, they will accumulate in lymph nodes, producing hypointense signals.[35] Unlike normal lymph nodes, metastatic nodes lack macrophages, they appear isointense in comparison with the pre-contrast stage. Therefore, the USPIOs are potentially useful in detecting lymph node metastases.[36]

Taking advantage of the long blood circulation of USPIO, Cheon *et al.* reported in vivo human breast tumor detection by using a magnetism-engineered Fe_3O_4 nanoparticle-herceptin probe.[37] Our group also reported the detection of human colon carcinoma xenografts implanted in nude mice by using monoclonal antibody-labeled Fe_3O_4 nanoparticles which were initially coated with poly(ethylene glycol) (PEG).[21] The PEG coating enables the Fe_3O_4 nanoparticles to evade the RES system. By a similar strategy, Sun *et al.* synthesized a c(RGDyK)-MC-Fe_3O_4

probe (MC: 4-methylcatechol) and used it in integrin $\alpha_v\beta_3$-rich tumor detection.[38] More examples of MRI tumor detection based on various types of targeting ligands such as proteins, peptides, aptamers and small molecules demonstrate that actively targeting the tumor *via* specific molecular recognition is becoming a very effective approach for early tumor detection.

3. Synthesis of superparamagnetic nanoparticles towards MRI applications

Superparamagnetism occurs when the size of a ferromagnetic material is so small that the ambient thermal energy is sufficient to induce the free rotation of the entire crystallite. Thus the material behaves in a manner similar to a paramagnetic material, except that the magnetic moment of the entire crystallite tends to align with the magnetic field. There exist different critical sizes for different types of spherical magnetic particles to transform from ferromagnetic or ferrimagnetic to superparamagnetic stages. For the most commonly used magnetic iron oxides in MRI, *i.e.*, Fe_3O_4, the critical size is 20–30 nm,[39] and a similar size also applies for γ-Fe_2O_3.[40]

Over the past three decades, the syntheses of magnetic nanoparticles have widely been investigated and different synthetic routes have been established ranging from physical methods such as mechanical grinding and biomineralization processes to chemical methods such as coprecipitation method, microemulsion method, hydrothermal synthesis, sol-gel synthesis, electrochemical method, sonochemical reaction, polyol method, flame-assisted method, thermal decomposition method, *etc*. In comparison with the physical methods and the biomineralization processes, the chemical methods, especially the solution-based synthetic routes, are generally more suitable for producing superparamagnetic iron oxide particles towards MRI applications, because they exhibit great advantages in controlling the following parameters, *i.e.*, particle size, particle size distribution, crystallinity degree, and phase purity, which are the most essential parameters in terms of MRI applications. Regarding the single-core contrast agents, the particle size and size distribution controls are extremely important for revealing the particle size-dependent biological distributions, pharmacokinetics, and elimination pathways, which remain less known, partly due to the poor availability of mono-dispersed particle samples with identical surface chemical structures for different sizes of interest, while the high crystallinity degree and phase purity are directly associated with the MRI contrast enhancement effects.[37] Last but not least, the surface chemical modifications also play an important role governing the fates of the magnetic nanoparticles in vivo apart from providing the underlying particles with the necessary water-solubility and colloidal stability under physiological conditions, which will be discussed in more detail in the following section. As the magnetic cores are the functional parts of magnetic particle-based MRI contrast agents, in this section we are mainly discussing the "core" synthesis.

According to chemical principles, the solution-based synthetic methods for producing superparamagnetic iron oxide nanoparticles can roughly be classified into two categories, *i.e.*, hydrolytic routes and non-hydrolytic routes. The hydrolytic synthetic routes, such as coprecipitation method, microemulsion method, hydrothermal synthesis, sol-gel synthesis, electrochemical method and sonochemical method, principally rely on the hydrolysis of ferric ions and ferrous ions, while the thermal-decomposition method as a main-stream non-hydrolytic synthetic technique relies on the pyrolysis of iron-organic compounds. Herein, we classify the synthetic routes in this way because water molecules present very strong affinities to ferric ion and ferrous ion. In addition, hydroxyl ions also present a very strong affinity to ferric ion and a medium affinity to ferrous ion. The presence of a great excess of water in the hydrolytic routes therefore results in very complicated surface binding situations involving water and hydroxyl ions, which not only affect the surface coating of stabilizing agents, but also vary the particle surface charge density and surface chemical composition.[41] Moreover, water as the reactant of the hydrolysis reactions of metal ions can induce very complex particle surface dynamics which strongly influence the particle size, size distribution, and even particle shapes, leading to poorly-defined morphologies including broad particle size distribution. In contrast, bulk water is not present in the non-hydrolytic synthetic routes, which is very helpful for eliminating the disadvantages of the hydrolytic synthetic methods.

There are certainly many methods in the literature suitable for producing magnetic iron oxide particles, herein we only focus on the methods by which the particles synthesized are readily dispersible in liquid media.

3.1 Hydrolytic synthetic routes

3.1.1 Coprecipitation method. Among the hydrolytic synthetic routes, the coprecipitation technique is the most important and widely used method. Almost all iron oxide-based MRI contrast agents which have been approved for clinical applications or at different pre-clinical stages are exclusively fabricated by this method. In fact, the hydrolytic synthetic routes for magnetite can be found in very early literature. In 1925, Welo *et al.* reported a synthetic route for producing magnetite by coprecipitating Fe(II)/Fe(III) in aqueous solutions.[42] In 1956, David *et al.* further developed the coprecipitation method by partial oxidation of a Fe(II) salt solution with KNO_3 under alkaline conditions at 90 °C.[43] Upon using a similar strategy, magnetite was also obtained by partial reduction of Fe(III) salt in alkaline solution.[44] Based on these chemical approaches, different hydrolytic synthetic routes were developed later on. As for γ-Fe_2O_3, it can be obtained by further oxidizing Fe_3O_4 nanoparticles under different conditions.[45,46] Because Fe_3O_4 has a higher saturation magnetization than γ-Fe_2O_3, it is more preferable for MRI application, but γ-Fe_2O_3 is more chemically stable under ambient conditions.

The preparation of magnetic iron oxide particles is very similar to that for bulk magnetite except that the growth of nuclei needs to be effectively inhibited so as to obtain nanometer-sized particles. Therefore, different types of polymers and small molecules are often used as precipitating agents which are also called surface capping agents or stabilizing agents, from the viewpoints of surface modification or colloidal stability, respectively.

According to the Lewis acid–base concepts as well as the classification of hard and soft acids and bases (HSAB), the iron atom on the magnetic iron oxide surface is a hard Lewis acid, while compounds containing O or N atoms, such as water,

alcohols, ethers, ketones, NH_3, amines, imines are hard Lewis bases. Therefore, based on the HSAB theory, namely hard acids reacting faster and forming stronger bonds with hard bases and vice versa, it can be deduced that water-soluble organic compounds bearing hard Lewis base groups can be used as precipitating agents (surface capping agents).

The polymer coating can generally be realized by two different strategies, *i.e.*, to coat the particles with polymers after precipitation or to directly synthesize iron oxide particles in the presence of polymers. Elmore reported an early example on dextran-coated ferromagnetic colloid *via* the precipitation method in 1938 by the first strategy,[47] while Cox *et al*. reported an iron-dextran complex in 1965 prepared by the second strategy.[48] These early investigations provided a solid foundation for the iron oxide contrast agents commercialized later on, as shown in Table I.

In general, biopolymers such as carbohydrates (dextran, chitosan, alginate, arabinogalactan), proteins, *etc*., and synthetic polymers such as PEG, poly(vinyl alcohol) (PVA), poly(acrylic acid) (PAA), poly(methylacrylic acid) (PMAA), poly(lactic acid), polyvinylpyrrolidone (PVP), polyethyleneimine (PEI), AB and ABC-type block copolymers containing the above polymers as segments are often used as precipitating agents.

However, the adsorptions of these polymers are usually pH-dependent,[49–51] which suggests that the electrostatic interactions may play an important role in coating the resultant nanoparticles. As magnetite is an amphoteric solid, magnetite nanoparticles present a pH_{PZC} (pH at the point of zero charge, PZC) of 6–8, determined by a potentiometric titration method.[52,53] Below pH_{PZC}, protonation of the particle surface leads to the formation of $\equiv Fe–OH_2^+$ moieties, while deprotonation occurring above the isoelectric point gives rise to $\equiv Fe–O^-$ surface moieties,[53] which affect the electrostatic attachments of the aforementioned polymers on the magnetic iron oxide particles.

Apart from the electrostatic interaction, ligand exchange (surface complexation), hydrophobic interaction, entropic effect, hydrogen bonding, and cation bridging were also reported to be responsible for the adsorption of stabilizing agents on the surface of iron oxides. Gu *et al.* reported systematic investigations on the mechanisms of adsorption and desorption of natural organic materials such as humic and fulvic acids which are representative natural organic materials.[54] By measuring the heat of adsorption of the organic substances on iron oxide by a microcalorimetry method, in combination with FTIR and ^{13}C NMR analysis, they demonstrated that a ligand exchange mechanism is responsible for the adsorption of humic and fulvic acids on iron oxide, at least at pH below pH_{PZC}, rather than electrostatic adsorption. Furthermore, they proposed a modified Langmuir model, in which a surface excess-dependent affinity parameter was defined to account for a decreasing adsorption affinity with surface coverage due to the heterogeneity of the natural organic materials and adsorbent surfaces. In that model, a hysteresis coefficient, h, is used to describe the hysteretic effect of adsorption reactions that, at $h = 0$, the reaction is completely reversible, whereas at $h = 1$, the reaction is completely irreversible. The fitted values of h for natural organic materials desorption on iron oxide surfaces range from 0.72 to 0.92, suggesting that the adsorbed natural organic material is very difficult to desorb. Humic and fulvic acids are rich in carboxylic acid and phenolic hydroxyl functional groups.[54] Their further investigations on substituted benzoic acids/phenols reveal that carboxyl functional groups are more active or more important than hydroxyl groups; however, when the hydroxyl group is ortho-positioned with respect to the carboxyl groups, the hydroxyl group and carboxyl group will simultaneously coordinate with the iron atom forming a mononuclear chelating complex structure.[55] Following that, they further demonstrate that PAA (Mw 2000) has stronger adsorption affinity than humic acid for the iron oxide surface.[49]

Because carbohydrates are abundant in hydroxyl groups as well as carboxylic groups (in alginate) and amino groups (in chitosan), therefore they can firmly stick to the particle surface and effectively inhibit the growth of crystal nuclei according to the adsorption mechanism mentioned above. Among carbohydrates, dextran is the most commonly used biopolymer in commercialized MRI contrast agents. Dextran is a branched polysaccharide made of many glucose molecules joined into chains of varying lengths (from 10 to 150 kilodaltons). The straight chain consists of α-1,6-glycosidic linkages between glucose molecules, while branches begin from α-1,4-linkages (and in some cases, α-1,2- and α-1,3-linkages as well). Dextran is used as an antithrombotic (anti-platelet) and to reduce blood viscosity in clinical applications. Apart from carbohydrates, denatured proteins may also be useful for coating magnetic iron oxide particles.[56]

Apart from polymers, small molecules such as citric acid, tartaric acid, gluconic acid, dimercaptosuccinic acid and phosphoryl choline are also useful precipitating agents for magnetic iron oxide particles.[57–61] In general, the surface attachment of these carboxylic acids also follows the ligand-exchange (surface complexation) mechanism due to the fact that citric, tartaric, and gluconic acids are α-hydroxyl acids and structurally similar to 2-hydroxybenzoic acid. Therefore, they act as chelating agents by firmly absorbing on the magnetic particles *via* surface complexation, eventually leading to the formation of nanometer-sized iron oxide particles. In addition, the surface complexation can effectively be used to tune the particles size.[57] For example, Bee *et al*. demonstrated that the average diameter of citrate-coated nanoparticles can be varied from 3 nm to 8 nm by decreasing the amount of citrate ions.[46] Although the chelating organic anions and polymer surface complexing agents can be used to tune the particle size, a reduced crystallinity degree is observed with increasing concentration of citric acid as a side effect.[62] Nevertheless, the citrate-coating strategy has successfully been used for a preclinical MRI contrast agent, *i.e.*, VSOP-C184.

As a matter of fact, Massart's early pioneering work demonstrated that the magnetic particles can even be synthesized in the absence of organic surface capping agents and subsequently form a stable magnetic colloidal solution in the alkaline range.[63] In later investigations, the influences of the following parameters on the yield of the coprecipitation reaction, diameter and polydispersity of the resultant nanoparticles were carefully investigated, *i.e.*, type of base (ammonia, CH_3NH_2 or NaOH), pH value, cations ($N(CH_3)_4^+$, $CH_3NH_3^+$, NH_4^+, Na^+, Li^+, K^+), and Fe^{2+}/Fe^{3+} ratio. Under optimized conditions, the average particle size can be tuned in the range 4–16 nm.[64] Massart's process has paved a successful synthetic route for producing aqueous magnetic fluids, making the coprecipitation technique a booming area later on. Nevertheless, the alkaline pH (>9) used for producing "naked" magnetic iron oxide particles will

undoubtedly facilitate the formation of iron hydroxide impurities.[46] Therefore, various types of stabilizing agents are used in producing MRI contrast agents for effectively tuning the pH_{PZC} far away from neutral pH so as to obtain colloidally stable iron oxide particles at physiological pH, and in the meantime avoid the formation of unwanted iron hydroxide impurities.

In general, the coprecipitation technique is a rather complex approach, not only because the complicated hydrolysis equilibria of ferric ions and ferrous ions are involved, but also because the shape, size and size distribution of the resultant nanoparticles are strongly influenced by a large number of synthetic parameters such as pH, concentrations of iron salts, ratio of Fe^{2+}/Fe^{3+}, counter ions of the cationic metal ions, reaction temperature, ionic strength of the medium, *etc*. Moreover, the type of precipitating agent for inhibiting the growth of the crystal nuclei also have strong impacts on the shape, size and size distributions. Consequently, the magnetic nanoparticles prepared *via* the coprecipitation method are typically characterized by broad size distributions greater than 50%.[65] Further particle size-sorting procedures can suppress the particle size distribution to 5% by successively precipitating particles of different sizes upon the use of various types of electrolytes, depending on the particle systems.[66] Apart from the broad size distribution, the synthesis has to be performed in controlled atmosphere to avoid unwanted oxidation. In spite of these intrinsic problems associated with a large number of kinetic factors, the well-documented method still allows mass production of magnetic iron oxide particles with good reproducibility for MRI purposes.

3.1.2 Other hydrolytic methods. Given that the particles obtained by the coprecipitation method possess broad size distributions, other methods are being developed for producing nanoparticles with uniform sizes.

The microemulsion method is a good choice regarding size control in general as it allows the chemical reactions for generating nanomaterials only to take place in constrained cavities, namely, aqueous microdroplets in oil, so as to suppress the particle size distribution. By modulating the parameters of the aqueous droplets the particle size and even shape can further be varied.[67] One of the disadvantages of the microemulsion method is related to the complicated purifying procedures required for removing the surfactants used for emulsifying the immiscible systems. Apart from that, the yield of nanoparticles is low compared with the coprecipitation method, limited by the narrow working window for microemulsions.[7]

Hydrothermal synthesis is based on aqueous reactions taking place under high pressure and temperature. It has become an important synthetic technique for producing magnetic nanomaterials such as ferrites. Recently, an important improvement has been made by Li *et al.* in producing monodispersed inorganic nanocrystals.[68] By skillfully utilizing the phase transferring processes established at liquid (ethanol-linoleic acid)/solid (metal linoleate) and solid/solution (water-ethanol) interfaces in combination with reduction reaction occurring in the vicinity of solid/solution interface and in-situ particle surface coating, they obtained monodispersed noble metal nanoparticles and further successfully applied the proposed "liquid-solid-solution" mechanism to the syntheses of a huge varieties of particles including magnetic iron oxides. It is therefore reasonable to expect promising results based on this synthetic route towards MRI applications, as an alternative approach to the coprecipitation method and the thermal decomposition method mentioned below. Although water is present in this synthetic route, it cannot simply be classified as a hydrolytic route as more complicated liquid phase-related processes are involved.

Other methods such as sol-gel process, electrochemical method and sonochemical reactions were also reported in the syntheses of magnetic iron oxide particles. The sol-gel process is more suitable for producing powders of magnetic particles,[69] it is therefore not very suitable for producing MRI contrast agents. The electrochemical method however does not differ very much from the coprecipitation method except that in the electrochemical approach ferric ions are generated by a sacrificial iron anode.[70] The hydrolysis and precipitation reactions follow those occurring in the coprecipitation process. The sonochemical reactions in most cases adopted volatile organometallic precursors such as $Fe(CO)_5$. Although both Fe_3O_4 and Fe_2O_3 nanocrystals can be prepared, the size distribution remains to be narrowed and the particle size tunability is worse.[71,72]

3.2 Non-hydrolytic synthetic routes

Non-hydrolytic synthetic routes include thermal decomposition method, polyol method, flame-assisted synthesis *etc*. Among these non-hydrolytic synthetic routes, the thermal decomposition method based on the pyrolysis of organometallic compounds, metal-surfactant complexes and metal salts has become the most successful approach for producing high quality iron oxide nanocrystals with perfect monodispersity, high crystallinity degree, satisfying size tunability, and better defined particle surface complexation structures.

3.2.1 Thermal decomposition in non-polar solvents. About 10 years ago, Alivisatos' group first developed the thermal decomposition method for producing mono-dispersed γ-Fe_2O_3, Mn_3O_4, and Cu_2O nanocrystals by pyrolyzing metal cupferron complexes M^xCup_x (Cup: N-nitrosophenylhydroxylamine, $C_6H_5N(NO)O^-$; M: Fe^{3+}, Cu^{2+}, Mn^{2+}) in trioctylamine at 200–300 °C.[12] Octylamine was used as the surfactant for γ-Fe_2O_3 nanocrystals. Uniform γ-Fe_2O_3 nanocrystals of 6.7 ± 1.4 nm were successfully obtained *via* a "hot-injection" method (*i.e.*, a stock solution of the metal precursor is quickly injected into the hot solvent) at 300 °C followed by reflux at 225 °C. A size-fractioning process was used to narrow the particle size distribution to <10%. Fig. 2a presents a typical TEM image of the as-prepared γ-Fe_2O_3 nanocrystals. Upon lowering the injection temperature or the injected precursor concentration, smaller nanocrystals were obtained. This pioneering work set the first successful example for achieving high quality iron oxide nanocrystals *via* a non-hydrolytic synthetic route.

Hyeon *et al.* further developed the above-mentioned synthesis by using $Fe(CO)_5$ instead of metal cupferron complexes in producing monodispersed γ-Fe_2O_3 nanocrystals.[13] As the pyrolysis of $Fe(CO)_5$ generated iron nanoparticles, an oxidation by trimethylamine oxide was used to further generate γ-Fe_2O_3 nanocrystals. The biggest advantage of this approach is that the resultant nanocrystals present a very narrow size variation of 5% so that no following size-selective process is required. By varying

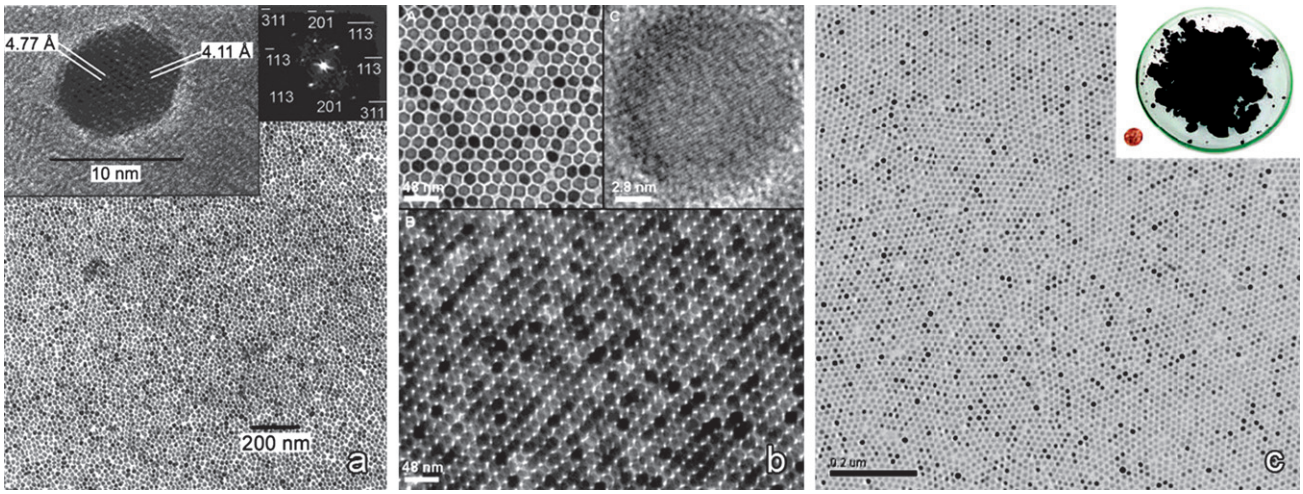

Fig. 2 a) γ-Fe_2O_3 nanocrystals synthesized by thermal decomposition of $FeCup_3$; b) Fe_3O_4 nanocrystals prepared by pyrolyzing $Fe(acac)_3$; c) magnetic iron oxide nanocrystals prepared by using iron oleate as precursor. (Images a, b, and c are reprinted from ref.12, 16, and 15, respectively, with permissions.)

the molar ratio of $Fe(CO)_5$ to oleic acid which serves as stabilizing agent, the size of the resultant nanocrystals can be tuned in a size range of 4–11 nm. However, larger γ-Fe_2O_3 nanocrystals (16 nm) were obtained only by seed-mediated growth. By a similar process, Woo *et al.* reported the synthesis of γ-Fe_2O_3 nanocrystals which were formed by consecutively aerating the reaction system at an appropriate temperature.[73] In addition, they demonstrated that higher oleic acid : $Fe(CO)_5$ ratios favor the formation of larger particles. However, when the molar ratio reached 3 : 1, 19 nm Fe_3O_4 rather than γ-Fe_2O_3 nanocrystals were generated. Cheon *et al.* further demonstrated that by pyrolyzing $Fe(CO)_5$ in ortho-dichlorobenzene containing dodecylamine (DDA) at 180 °C under aerobic conditions, the shape of γ-Fe_2O_3 nanocrystals can also be varied: for example, 12 nm nanocrystals with diamond (~40%), triangle (~30%) and spherical (~30%) shapes could be obtained.[19] Further increasing the molar ratio of DDA : $Fe(CO)_5$ from 1 : 1 to 10 : 1 led to the formation of larger particles of 40 nm as well as smaller ones of 10 nm after 9 h of injection. Prolonged reaction of 16 h further increased the size of the larger particles to 50 nm, while the smaller ones greatly decreased in both quantity and size, which was interpreted to be a result of Ostwald ripening.[19]

Sun *et al.* reported the synthesis of monodispersed Fe_3O_4 nanoparticles with sizes below 20 nm by the thermal decomposition method for the first time in 2002.[16] In their synthesis, iron(III) acetylacetonate ($Fe(acac)_3$) was adopted instead of metal cupferron or $Fe(CO)_5$. The thermal decomposition of $Fe(acac)_3$ was carried out in phenyl ether in the presence of 1,2-hexadecanediol, oleic acid, and oleylamine to produce size-controlled Fe_3O_4 nanoparticles as shown in Fig. 2b. In addition, the "hot injection" was abandoned. Instead, a "heating-up" method was used, *i.e.*, heating up the solution consisting of all reactants to designed temperatures. They further found that higher reaction temperatures favor larger particle formation.[17] For example, by replacing the phenyl ether (boiling point 259 °C) with benzyl ether (boiling point 298 °C), the particle size is increased from 4 nm to 6 nm. The author claimed that the key to the success of making monodispersed nanoparticles is to heat the mixture to 200 °C first and maintain this temperature for some time before it is heated to reflux. They also demonstrated that 1,2-hexadecanediol is better, with respect to particle quality and product yield, than stearyl alcohol and oleyl achohol. Although the reaction mechanism for the formation of Fe_3O_4 was not elucidated, they did observe FeO in the early stages (5 min) of the preparation appearing as intermediate species.

Based on the pyrolysis of metal fatty acid salts, Peng *et al.* reported a simple, reproducible, and general method for preparing magnetic oxide nanocrystals.[18] The particle sizes can be controlled between 6 nm and 50 nm by varying the amount of excess fatty acid or by changing the concentration of the precursor salt following the "heating-up" method.[18] It was further demonstrated that higher excess of fatty acid favors larger particles. In contrast, the presence of amines and alcohols as activating reagents leads to the formation of smaller particles. The current synthetic approach, characterized by the safety and air-stability of the metal fatty acid salts, was further demonstrated to be a facile method for producing monodispersed magnetic nanocrystals (Fig. 2c) at an ultra-large-scale (tens of grams) by Hyeon *et al.*[15] The investigations of Hyeon *et al.* demonstrate that reaction temperature is a very effective tool for achieving nanocrystals of different sizes, such as 5 nm (274 °C), 9 nm (287 °C), 12 nm (317 °C), 16 nm (330 °C) and 22 nm (365 °C). Moreover, the concentration of oleic acid can further be used to finely tune the particle size in a range of 11–14 nm at 320 °C. Further TEM investigations suggested that with a constant heating rate of 3.3 °C/min no particles were produced at 310 °C and 8–11 nm particles were generated when the temperature reached 320 °C. At 320 °C, the particle size remained unchanged against reaction time between 10 and 30 min. In contrast, reaction at 260 °C for one day produced polydispersed and poorly crystalline particles of 9 nm and 3 day reaction generated monodispersed 12 nm particles. Lowering the aging temperature to 240 °C resulted in no particles for one day and highly polydispersed 14 nm particles in 3 days. Further lowering the reaction temperature to 200 °C gave rise to no particles in 3 days. From the above experiments, the authors drew the conclusion that the

nucleation occurs at 200–240 °C initiated by the dissociation of one oleate ligand and the major growth occurs at ~300 °C initiated by the dissociation of the other two oleate ligands, and they also claimed that the key to the synthesis for achieving monodispersed nanocrystals is to separate the nucleation and growth processes.[4,15]

By using iron tris-2,4-pentanedionate ($Fe(acac)_3$) as precursor, Cheon *et al*. reported a series of metal-doped magnetism-engineered iron oxide (MEIO) nanoparticles of spinel MFe_2O_4 (M = Mn, Fe, Co or Ni), M was provided by metal chloride in the reaction systems.[37] Among them, $MnFe_2O_4$ present improved saturation magnetization which is helpful for further increasing the imaging contrast of MRI in comparison with Fe_3O_4.[37]

Apart from metal-organic complexes, inorganic compounds can also be used as iron source precursors. Colvin and co-workers used FeOOH as a precursor to prepare high quality Fe_3O_4 nanocrystals (12.5 nm) by taking advantage of the good solubility of FeOOH in oleic acid.[74] They also demonstrated that higher concentration and temperature generally favor the formation of larger particles of 20–30 nm but at the cost of monodispersity.

3.2.2 Thermal decomposition in strong polar solvents. The above mentioned investigations make the thermal decomposition synthesis a powerful method for producing magnetic iron oxide nanocrystals with high quality in terms of crystallinity degree, particle size distribution, and particle size tunability. Furthermore, the thermal decomposition method is easily scaled up for mass production. Most importantly, the resultant nanocrystals in most cases lie in the size regime very suitable for MRI applications. Despite these remarkable advantages over the hydrolytic synthetic routes, the products of the syntheses mentioned above cannot directly be used at the single particle level due to the surface-coated long alkyl chain surfactant molecules which make the nanocrystals more readily dissolvable in organic solvents such as hexane, chloroform, toluene, *etc*.

Another common feature of the above-mentioned syntheses is the use of non-polar solvents such as phenyl ether, benzyl ether, trioctylamine, octyl ether, octadecene, 1-hexadecene, 1-eicosene, ortho-dichlorobenzene, *etc*., as reaction medium. In order to produce aqueous dispersible magnetic nanocrystals which inherit the advantages of the thermal decomposition method, we replaced the non-polar solvent with strongly polar 2-pyrrolidone in our first attempt.[23] We chose 2-pyrrolidone because its boiling point (245 °C) can guarantee the thermal decomposition of organometallic precursors such as $Fe(acac)_3$. Moreover, 2-pyrrolidone is a strong polar solvent which can mix well with water in almost at any ratio. By directly pyrolyzing $Fe(acac)_3$ in 2-pyrrolidone, we obtained iron oxide nanocrystals of 5 ± 1.2 nm. Larger particles of 11 ± 2.5 nm were prepared by seed-mediated growth. Further titration experiments demonstrate that the resultant nanocrystals are stoichiometric Fe_3O_4 (Fe^{2+}:Fe^{3+} = 1:2) rather than Fe_2O_3, in good agreement with the X-ray diffraction results. These nanocrystals are dispersible in both acidic and alkaline media, but not at neutral pH, suggesting that these nanoparticles become dispersible by charging the particle surface. X-Ray photoelectron spectroscopy (XPS) experiments reveal that 2-pyrrolidone not only provides a high temperature environment for the decomposition of $Fe(acac)_3$, but also serves as a surface capping agent by coordinating with the surface Fe atom *via* its carbonyl group.

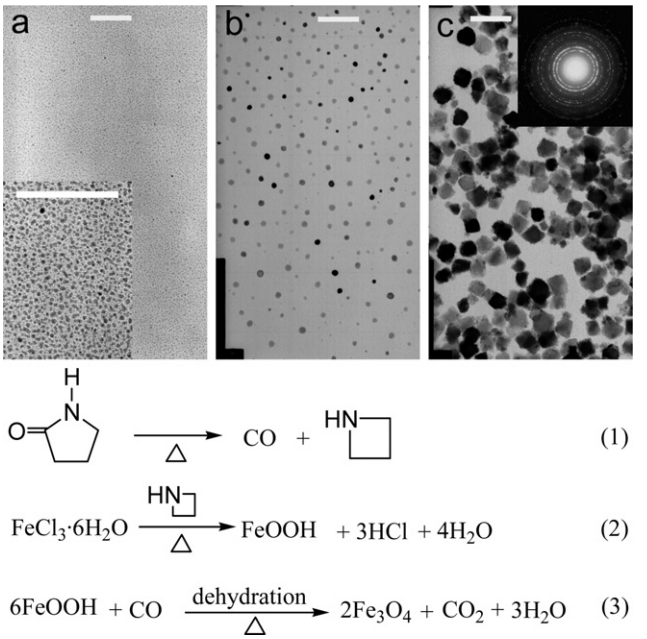

Fig. 3 TEM images of Fe_3O_4 nanocrystals obtained after refluxing 2-pyrrolidone containing $FeCl_3 \cdot 6H_2O$ for 1, 10 and 24 hours (from left to right). The scale bar corresponds to 100 nm (also for inset). The mechanisms for the formation of Fe_3O_4 nanocrystals are shown below. (Reprinted from ref. 24 with permission.)

To make the synthesis greener, $FeCl_3 \cdot 6H_2O$ was adopted as precursor in our second attempt towards aqueous dispersible Fe_3O_4 nanocrystals.[24] Simply by boiling a 2-pyrrolidone solution of $FeCl_3 \cdot 6H_2O$, we obtained Fe_3O_4 nanocrystals of different sizes, *i.e.*, 4 nm, 12 nm, and 60 nm. The particle size was controlled by the reflux time, as shown in Fig. 3. As a matter of fact, the Fe_3O_4 phase often appears in non-polar reaction systems solely upon the pyrolysis of trivalent Fe compounds.[17,18] Therefore, it is important to know how Fe^{2+} is generated. With respect to the specific system of $FeCl_3 \cdot 6H_2O$/2-pyrrolidone, ultra-violet photoelectron spectroscopy was used in combination with an identification reaction to analyze the small molecular weight species released during the reaction. Based on the identification results, a mechanism for the formation of Fe_3O_4 was proposed as shown in Fig. 3. 2-Pyrrolidone undergoes slow thermal decomposition at its boiling point generating CO and azetidine; catalyzed by azetidine $FeCl_3 \cdot 6H_2O$ is hydrolyzed forming FeOOH which is soluble in the system; the dehydration of FeOOH in the presence of CO leads to the formation of magnetite.[24]

Although the 2-pyrrolidone-based preparations offer a simple approach towards aqueous dispersible Fe_3O_4 nanocrystals and inherit the advantages of the thermal decomposition syntheses carried out in non-polar solvents, the poor solubility of the resultant particles around neutral pH remains an obstacle for further exploring their in vivo applications. To solve this problem, we pyrolyzed $Fe(acac)_3$ in 2-pyrrolidone in the presence of monocarboxyl-terminated poly(ethylene glycol) (MPEG-COOH).[20–22] PEG is a very good choice in terms of

biocompatibility. As carboxylate groups can firmly bind to the particle surface, the PEG-modified Fe_3O_4 nanocrystals obtained exhibit excellent aqueous solubility not only in pure water but also in physiological saline, which allows us to further use these PEG-coated Fe_3O_4 nanocrystals in disease detection.[75] α,ω-Dicarboxyl-terminated PEG(HOOC-PEG-COOH) was further used instead of MPEG-COOH to prepare biocompatible Fe_3O_4 nanocrystals with surface reactive moieties.[20] The surface carboxylate residues can be used for further covalently conjugating the biocompatible Fe_3O_4 nanocrystals to an anti-tumor antibody, forming a tumor specific MR molecular probe.[21]

Recently we further developed the thermal decomposition syntheses carried out in strong polar solvents by replacing 2-pyrrolidone with N-vinyl-2-pyrrolidone (NVP).[25] In general, PVP-coated Fe_3O_4 nanocrystals are prepared by pyrolyzing $Fe(acac)_3$ in NVP at 200 °C *via* a "one-pot" reaction. In this preparation, $Fe(acac)_3$ acts not only as the iron precursor but also as an initiator for the polymerization of NVP, while NVP provides the high reaction temperature for pyrolyzing $Fe(acac)_3$ in addition to serving as a coordinating agent which is polymerized in situ forming the PVP-coating layer. The resultant PVP-coated Fe_3O_4 nanocrystals present super-dissolvability not only in water and PBS but also in 10 different types of organic solvent.

The above-mentioned syntheses perfectly combine particle synthetic chemistry with surface chemistry and allow the preparation of water soluble, biocompatible, and even surface reactive moiety-bearing biocompatible Fe_3O_4 nanocrystals *via* "one-pot" reactions.

3.2.3 Growth mechanism of the particles prepared by the thermal decomposition method. The particle size distribution is an important criterion for evaluating the quality of an ensemble of nanocrystals due to the strongly size-dependent properties. With respect to magnetic iron oxide nanoparticles, the thermal decomposition approach seems to be the best in terms of particle size uniformity in comparison with the classic synthetic methods, apart from providing a high crystallinity degree enabled by the high boiling point solvents. Therefore, it is important to discuss the growth mechanism for the magnetic nanocrystals generated by the thermal decomposition method.

According to classic colloid theory, the growth of colloidal particles from initially supersaturated solution undergoes nucleation, growth and solid-phase formation *via* agglomeration of small crystal grains. In the 1950s, LaMer *et al.* proposed a strategy for achieving monodispersed colloids.[76] According to his model, the repetitive nucleation should be made so short that no additional nucleation occurs; consequently, monodispersed colloidal particles are formed *via* uniform growth on the existing nuclei. Based on the LaMer model, Bawendi *et al.* firstly invented a "hot-injection" method in order to make the reaction quickly enter stage II of the LaMer plot to achieve "burst-nucleation".[77] The "hot-injection" method was then widely used in preparing mono-dispersed fluorescent CdSe Q-dots[78] and magnetic iron oxide particles as well.[12] Hyeon *et al*. adopted this LaMer model to further interpret the homogenous nucleation of magnetic nanocrystals occurring in the thermal decomposition synthesis, but he also admitted that the underlying mechanism for the "heating-up" method remained not very clear because the latter method seems to offer comparable or even better quality magnetic nanocrystals in terms of particle size uniformity.[4] Hyeon *et al*. further performed numerical simulations for both "burst of nucleation" and crystal growth. In his theoretical model of particle growth, he combined the "focusing" effect ("focusing of size distribution") and the "defocusing" effect to explain the acquisition of mono-dispered nanocrystals.[4] The "focusing" and "defocusing" effects were initially used by Peng *et al*. to explain the growth CdSe Q-dots.[78]

According to the "diffusion-controlled" model[78] which is believed to be responsible for high quality nanocrystals,[79] if the average distance between the particles is large enough, the diffusion layer formed at the periphery of each particle is undisturbed. When the concentration of monomer in bulk solution is higher than the solubility of all crystals, the amount of monomers diffused into the diffusion sphere and subsequently deposited on the crystal surface should depend on the surface area of the diffusion sphere rather than the size of the nanocrystals, meaning that the volume of every crystal increases at the same rate. Thus, smaller crystals grow faster than larger ones in terms of diameter, leading to the kinetically controlled "focusing" effect.[78,80] However, according to the Gibbs-Thomson theory, smaller crystals also possess higher surface energies or chemical potentials which drive them to grow faster to minimize the surface energies, leading to a thermodynamically controlled "focusing" effect, which is typically regarded as a "growth-controlled" mechanism. However, an opposite effect also occurs, especially when the monomer concentration in bulk solution is lower than the solubility of small nanocrystals but higher than the larger ones in the solution, small particles consequently decrease in size and large ones will grow larger, giving rise to an Ostwald ripening process.[4,78,80,81] In the classic Ostwald ripening model, smaller particles dissolve to form monomers which serves as growth materials for larger particles. Consequently, the standard deviation of the particle size distribution becomes broader.

From these theoretical discussions, it is safe to conclude that to effectively shorten the repetitive nucleation period and to further enhance the "focusing" effect and depress the "defocusing" effect should be the most effective measures for preparing monodispersed nanocrystals. Experimentally, the "hot-injection" method seems to be an adequate measure as it induces the burst of nucleation, while adopting as dilute as possible monomer concentration, which is slightly higher than the solubility of crystal nuclei, should also be a correct measure for depressing the "defocusing" effect. Nevertheless, apart from these general rules, the following unique features of the thermal decomposition reactions should be taken into considerations for understanding the superior ability of the thermal decomposition syntheses in achieving mono-dispersed iron oxide particles.

1) The formation of nanocrystals by the thermal decomposition method is generally described by the processes shown in Fig. 4. In fact, the monomers used in the discussion of "focusing" and "defocusing" effects remain to be identified. They are believed to be active atomic or molecular species.[81] Moreover, little is known about the nuclei which should be soluble intermediate clusters formed by monomers.[82–89] Apart from that, the chemical transformation from precursor to monomer, the aggregation of monomers to form clusters, and the

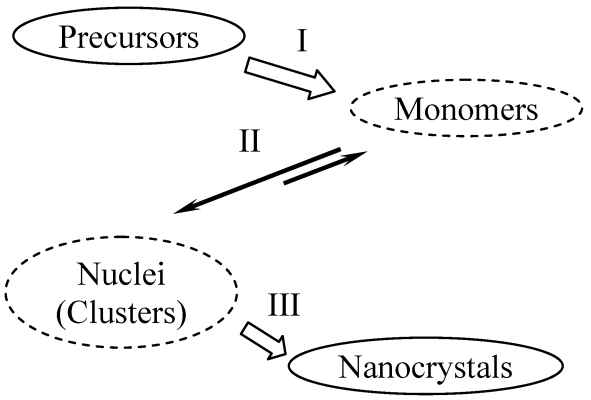

Fig. 4 Schematic drawing of the procedures for iron oxide nanocrystals growing in non-polar solvents *via* the pyrolysis of iron precursors. The monomers and nuclei remain to be identified. The decomposition of the chelating ligands, release of small molecular weight species, and indissolubility of the iron oxide species in non-polar solvents may make procedures I and III hardly reversible.

transformation of clusters to the final nanocrystals are less known as yet, and some of them may not be reversible.

2) With respect to the thermal decomposition of iron precursors, the release of small molecular species is often observed, which will greatly destroy the equilibria required for establishing the "defocusing" process. A number of mechanism investigations confirm that different types of small molecular weight species are released during the formation of magnetic iron oxide nanocrystals upon pyrolysis of various types of iron precursors. For example, water, CO, and CO_2 and azetidine are released from a very simple system of $FeCl_3 \cdot H_2O$ in 2-pyrrolidone;[24] while CO_2 is released from another simple system consisting of $Fe(oleate)_3$ and oleic acid in 1-octadecene.[15] From a relatively more complicated system of $Ni(acac)_2 \cdot H_2O$/3-aminopropyltrimethoxysilane/tetraethyloxysilane in 2-pyrrolidone, we also observed the release of CO_2, CH_3OH, and CH_3COCH_3 during the thermal decomposition of $Ni(acac)_2 \cdot 2H_2O$.[90] In addition, Sun also found FeO intermediate species formed in the system consisting of $Fe(acac)_3$, 1,2-hexadecanediol, oleic acid, and oleylamine in phenyl ether.[17] All these results suggest that the pyrolysis of metal precursors is very complicated involving different types of decomposition reactions and redox reactions. Moreover, the release of small molecular weight species as the byproducts of the reaction makes the thermal decomposition reactions hardly reversible, while the classic crystal growth theory considers the crystallization reaction merely as a solid-solute conversion process. Even if more complicated reactions can be adopted for producing nanoparticles,[76] all species necessary for establishing the dissolution and precipitation equilibria remain available in the reaction system rather than being expelled from the reaction system.

3) Under high reaction temperature, usually above 200 °C or even 300 °C (for example in octadecene), even if some simple metathesis reactions superficially occur in the metal-surfactant complex system,[79] the precipitation (for generating nanocrystal) and dissolution of iron oxide nanocrystals may hardly be reversible due to the generation of low boiling point species such as water which is required for maintaining the precipitation-dissolution equilibria. Some size distribution broadening effects were observed and used to support the "Ostwald ripening" process in the thermal decomposition synthesis,[19,79] but more careful experiments are required for excluding the repetitive nucleation by monitoring the conversion of the preparation while the particle size distribution is getting broadened, which to the best of our knowledge is not yet clarified with respect to magnetic iron oxide nanocrystals prepared by the thermal decomposition method.

4) The "defocusing" and "focusing" effects are widely used to interpret the formation of mono-dispersed nanocrystals. But these effects are based on the dissolubility of the nanocrystals. With respect to iron oxide, the binding force of Fe–O bond is as high as 397.5 kJ/mol, therefore, it is very hard to remove the Fe atom away from the particle surface in non-polar environments. In other words, the resultant iron oxide should be indissoluble in non-polar media.

All these discussions suggest that non-polar solvents are greatly unfavorable for the "defocusing" effect. Due to the indissolubility of iron oxide in non-polar solvents, the nuclei can only choose to grow faster to minimize the surface energy, largely following the thermodynamically controlled focusing effect (growth-controlled mechanism), eventually leading to the formation of mono-dispersed iron oxide nanocrystals, which interprets the fact that the overall size distribution of the as-prepared iron oxide nanocrystals through the thermal decompositions of various types of iron precursors is much narrower than those produced in aqueous systems in which kinetic factors largely govern the particle growth.

Moreover, the following experimental observations also suggest that the growth of iron oxide nanocrystals may follow the growth-controlled mechanism. Hyeon reported the successful control over the size of iron oxide by reaction temperatures, *i.e.*, 5 nm (274 °C), 9 nm (287 °C), 12 nm (317 °C), 16 nm (330 °C) and 22 nm (365 °C).[15] Furthermore, they also observed that the nanoparticles grew at 320 °C to 12 nm within 10 min and remained almost unchanged at prolonged reaction time (20 and 30 min), which suggests that within a very short time window, the nanocrystals can grow to a thermodynamically controlled size. Higher temperature enables the particle to grow further by more heavily activating the surface Fe-ligand bonding.[91] Our unpublished results on Fe_3O_4 nanocrystals, prepared by thermally decomposing $Fe(acac)_3$ in phenyl ether in the presence of oleylamine and carboxylated PEG, also suggest that the yield of the reaction is time dependent at certain temperatures, while the particle size is nearly unchanged within a time window of 1–24 h. However, it was found that the increased molar ratio of oleic acid to $Fe(oleate)_3$ is favorable for largely increasing the particle size,[18] which seems to be contradictory to our guess that the particle growth predominantly follows the growth-controlled mechanism. However, apart from encouraging the formation of the Fe_3O_4 phase,[18,73] an extra large ratio of oleic acid to $Fe(acac)_3$ will not only unavoidably alter the properties of the reaction media, but also largely increase the boiling point of the reaction system.

In fact, also doubted by Peng[80] and Hyeon *et al.*,[4] the overall nanocrystal growth models have some limitations as they are based on the classic crystallization concepts, such as the Gibbs-Thompson equation and Ostwald ripening, whose reliabilities are

highly questionable for inorganic nanocrystals such as iron oxide particles produced in non-polar solvents. We do not deny the efforts for suppressing the particle size distribution of iron oxide nanocrystals in literature by manipulating the synthetic parameters. We simply want to emphasize that the non-polarity of the solvents commonly used in the thermal decomposition method is unfavorable for the reversibility of the particle growth, consequently leading to the narrow particle size distribution no matter how the preparations are carried out, *i.e.*, by the "hot-injection" method or by the "heating-up" method, which is principally controlled by the intrinsic properties of the system, *i.e.*, inorganic nanocrystals growing in non-polar solvents. As for the strong polar solvent systems we developed,[22–25] one of the biggest advantages is that the strong polarity of 2-pyrrolidone allows the use of various types of surface ligands for facilely achieving biocompatible nanocrystals *via* a "one-pot" reaction.[20–22] Even though the strong polar solvent may encourage the "defocusing" effect, Fe_3O_4 nanocrystals with a slightly broader size distribution (~15%) can be obtained without applying any size-sorting treatment.[21–24]

Apart from the synthetic routes mentioned above, attention should be paid to the preparations of uniform nanoparticles under supercritical conditions[92] or in ionic liquids[93] which will not be discussed in this article.

4. Basic requirements for developing iron oxide-based contrast agents

The development of iron oxide-based contrast agents shown from left to right in Fig. 1 suggests that smaller size contrast agents generally favor more sophisticated applications due to their longer blood circulation time which is characterized by the blood half-time ($T_{1/2}$). Moreover, disease detection through iron oxide-enhanced MRI, especially tumor detection, is gradually shifting from passive targeting modes to active targeting modes by taking advantage of molecular recognition. To examine these developments from a chemistry viewpoint, producing iron oxide-based MR molecular probes capable of actively targeting disease requires the nanoparticles to possess water solubility, biocompatibility, colloidal stability under physiological conditions, and surface functionalizability in addition to small particle size.

4.1 Water solubility and colloidal stability

Herein, the water solubility of particles means that the nanoparticles can spontaneously be dissolved in aqueous media forming a thermodynamically stable solution of particles. The aqueous dissolvability of magnetic nanoparticles facilitates the subsequent chemical processing for MRI applications apart from being favorable for storage and transportation. The nanoparticles which can form colloidally stable sols principally do not need to have water solubility due to the fact that various types of forces can be used to achieve the colloidal stability of given particles. In principle, the colloidal stability of magnetic nanoparticles in aqueous media results from the equilibrium established between attractive and repulsive forces. Theoretically, attractive forces come from van der Waals forces, dipolar and magnetic dipolar forces, while repulsive forces mainly originate from electrostatic repulsion and steric repulsion. Therefore, electrostatic repulsion and steric repulsion can effectively be used for elaborating the colloidal stability.

For nanoparticles in aqueous media, the particle surface charges are balanced by an equal but oppositely charged region of counter-ions. Some of the counter-ions might specifically adsorb near the surface and build an inner sub-layer, or so-called stern layer. The outer part of the screening layer is usually called the diffuse layer. The diffuse layer, or at least part of it, can move under the influence of tangential stress, therefore a slipping plane is introduced to separate the mobile fluid from fluid that remains attached to the surface. The electric potential at this plane is called the electrokinetic potential or zeta potential, denoted as ζ-potential. A value of 25–30 mV (positive or negative) can be taken as the arbitrary value that separates low-charged surfaces from highly-charged surfaces. It is quite obviously that nanoparticles with highly charged surfaces more readily form stable sols.

For magnetic iron oxide particles to be colloidally stable in aqueous media at physiological pH (7.35–7.45 for human blood), to bring in additional charges to the particle surface is very important for electrostatically stabilizing the colloids due to the fact that the pH_{PZC} of "naked" iron oxide is around 7; otherwise they will flocculate. It was demonstrated that the attachment of small chelating agents on the surface of iron oxide particles can greatly shift the pH_{PZC} point of iron oxide particles away from neutral pH, in addition to effectively inhibiting the crystal growth.[94] Fauconnier *et al.* further demonstrated that the co-adsorption of gluconic acid and citric acid on γ-Fe_2O_3 particles gave rise to colloidal solutions stable within a wide pH window, 3.5–11.[59]

Nevertheless, satisfying colloidal stability around neutral pH is not enough for magnetic nanoparticles to be useful as MRI contrast agents administrated IV (intravenously), they should also have good enough colloidal stability at physiological ionic strength around 0.17 M. Phosphate buffered saline (PBS) is often used to mimic the pH and ionic strength of physiological conditions as the osmolarity and ion concentrations of the PBS buffer match those of the human body. Increasing the ion strength of the aqueous media will undoubtedly suppress the electric double layer around the charged particle, eventually leading to fluctuation of the colloids. Therefore, polymers are preferred as stabilizing agents as they provide steric repulsion to the nanoparticles in addition to electrostatic repulsion, consequently the influence of ionic strength on the colloidal stability can effectively be reduced. For example, superparamagnetic Fe_3O_4 nanoparticles synthesized by the coprecipitation method in the presence of poly(vinyl alcohol phosphate) were found to be stable at pH 5–8 for 4 weeks.[95] The PVP-coated Fe_3O_4 nanocrystals, prepared *via* a "one-pot" reaction, exhibited excellent solubility in water within a wide pH range and in PBS as well as 10 different types of organic solvents.[25]

Actually, under physiological conditions, apart from pH value and ion strength, the existence of a great variety of proteins has to be taken into consideration. Therefore, to effectively minimize the aggregation of the particles caused by protein adsorption also needs to be taken into consideration. Thus, anti-biofouling polymers are preferred to modify the magnetic nanocrystals for producing RES-evading particles with long blood half-times.[96] Among anti-biofouling polymers, PEG is one of the good

choices. We have demonstrated that PEG-coated Fe_3O_4 nanocrystals, prepared by thermal decomposition of $Fe(acac)_3$ in 2-pyrrolidone in the presence of MPEG-COOH, present a long blood circulation duration.[22] Apart from PEG, dextran is also a good choice for resisting protein adsorption.

As mentioned in the previous section, the thermal decomposition methods offer the best magnetic nanocrystals with narrow particle size distribution, high magnetic susceptibility and sufficient size tunability in the size regime interesting for MRI applications. Unfortunately, all magnetic iron oxide nanocrystals prepared through the thermal decomposition methods, except for those prepared with the use of strong polar solvents reported by us, are not water soluble. Therefore, the following different approaches have been developed for transferring the hydrophobic nanocrystals into water.

1) Nanocrystals capped by long hydrophobic chains are transferred into water *via* ligand displacement reactions. 2,3-Dimercaptosuccinic acid (DMSA) was used to prepare DMSA-coated Fe_3O_4 nanoparticles which are stably dispersible in PBS.[97,98] By a similar approach, dopamine was used to displace the hydrophobic ligand on the magnetic iron oxide particles because it can firmly coordinate with Fe forming a stable chelating complex.[99] The resultant dopamine-coated Fe_3O_4 nanocrystals are stable in water and PBS as well. This method can also be used to prepare aqueous dispersible magnetic nanocrystals with core-shell structures, *e.g.*, $Fe@Fe_3O_4$[100] and $Co@Fe_2O_3$,[101] and alloy structures, *i.e.*, FePt.[102] According to the investigations on the surface complexation of iron oxide nanocrystals,[46,58,103] small chelating agents are not limited to the above-mentioned molecules. Nevertheless, a major difficulty may come from how to control and characterize the displacement degree of the ligands.

2) Nanocrystals capped by long alkyl chain molecules are transferred into water *via* phase transferring agents. Typically, the transferring reagents consist of long hydrophobic chains. Upon the hydrophobic interaction of the incoming long hydrocarbon chain with that initially on the particle surface, the nanoparticles are rendered soluble in water upon the buildup of a "quasi"-interdigital bilayer structure on the particle surface with the hydrophilic head of the phase transferring agent pointing to the aqueous medium. Robinson *et al*. reported water soluble magnetic MFe_2O_4 (M = Fe, Co, or Mn) nanoparticles transferred into water by using a combination of alkylphosphonate surfactants and other surfactants such as ethoxylated fatty alcohols or phospholipids.[104] The resultant aqueous colloidal solutions were stable at pH 5 or 9. Bao *et al.* synthesized a pegylated phospholipid, 1,2-distearoyl-*sn*-glycero-3-phosphoethanolamine-*N*-methoxy(polyethylene glycol) 2000 (DSPE-mPEG 2000), and used it to transfer hydrophobic Fe_3O_4 nanocrystals into aqueous solution.[105] Although the transferring process resulted in slight agglomeration, the resultant nanoparticles were colloidally stable in water and 1 × PBS for a period of weeks at 4 °C. In contrast, polymeric surfactants bearing a number of long hydrocarbon chains seem to be more adequate for rendering the hydrophobic nanoparticles water soluble. The widely used polymeric phase transferring agents are based on commercial products, *e.g.*, poly(maleic anhydride-alt-1-tetradecene). Pellegrino *et al*. have developed a simple and general strategy for decorating hydrophobic nanocrystals such as Fe_2O_3, $CoPt_3$, CdSe@ZnS, and Au, to eventually render them dispersible in water and TBE (tris-borate-EDTA) buffer (pH 8–9).[106] The experiments are briefly described as follows. Poly(maleic anhydride-alt-1-tetradecene) was firstly coated on the particle surface, then partly cross-linked by bis(6-aminohexyl)amine in chloroform. After evaporation of the solvent, the resultant solid was redispersed in water or buffers forming colloidal solutions which were stable for months. Fluorescence correlation spectroscopy (FCS) was used to determine the hydrodynamic size of fluorescent CdSe@ZnS dots before and after being transferred into aqueous systems. A significant increase in particle size suggests that a polymer shell is successfully formed. Further electrophoresis experiments on the polymer-coated nanocrystals suggest that no interparticle agglomeration occurs during the phase transferring process.[106] By a similar approach, Yu *et al*. synthesized an amphiphilic polymer by grafting poly(maleic anhydride-alt-1-octadecene) (PMAO) with PEG 6000 for transferring Fe_3O_4 nanocrystals from organic solvents to aqueous systems.[107] The authors claimed that the resultant PMAO-PEG-coated Fe_3O_4 nanocrystals are colloidally stable in water over a wide pH range of 4–10, or in 10 × PBS or 1 M NaCl solutions (pH 6–8) for over two years. All these experiments strongly suggest that the steric stabilization effect from the polymer coating layer greatly favors colloidal stability over a large pH range even in the presence of salts, even though the use of polymeric phase transferring agents will increase the overall hydrodynamic size of the resultant nanoparticles.

4.2 Biocompatibility

Biocompatibility is one of the most important prerequisites for magnetic nanocrystals being used in vivo. The biocompatibility of a material refers to its ability to perform its desired function in a medical therapy without eliciting any undesirable local or systemic effects in the recipient of that therapy, but generating the most appropriate beneficial cellular or tissue response in that specific situation, and optimizing the clinically relevant performance of that therapy.[108] Biocompatibility is traditionally concerned with implantable devices that are intended to remain in an individual for a long time. Different from the implanted materials, iron oxide-based contrast agents are supposed to be eliminated from the body after exerting their contrast-enhancing function. Therefore, the toxicities of both iron oxide and coating materials, local or systemic effects, circulating behaviors and elimination pathways are the major concerns with respect to the developments of iron oxide-based contrast agents for MRI applications.

4.2.1 Toxicity. According to standard toxicological and pharmacological tests of several iron oxide contrast agents, iron oxide nanoparticles show a satisfactory safety profile for human use.[2] Actually, human tissues contain a certain amount of iron carried by haemosiderin, ferritin and transferrin. For instance, a normal human liver contains approximately 0.2 g Fe/kg wet weight and total human iron stores are approximately 3.5 g Fe/70 kg body weight. Investigations of the chronic iron toxicity show that cirrhosis and hepatocellular carcinoma developed only after the liver iron concentration exceeds 4 g Fe/kg wet weight.[109,110]

Regarding the coating materials, dextran and PEG with proper molecular weights are on the safe side. The former can be biodegraded within the body while the latter can easily be excreted.[111] However, the toxicities of the coating materials developed at the in-lab stage need to be further evaluated.

4.2.2 Local or systemic effects. The effects of iron oxide at cellular and sub-cellular levels are generally very complicated. An increase in oxidative stress was observed from RAW macrophages loaded with magnetic nanoparticles (VSOP C200) in in vitro experiments, which was caused by intracellular iron released from the loaded VSOPs. But the transient oxidative stress could be prevented by using antioxidants or iron chelators such as desferal. Further experiments suggested that the in vitro magnetic labeling of macrophages with VSOPs minimally affected cell growth and viability.[112]

Regarding the systemic effects, the presence of anti-dextran antibodies in a few individuals suggested at least a theoretical danger from dextran-coated contrast agents. It was reported that serious allergic reactions were caused, at least in part by dextran-reactive IgG antibodies when dextrans (40 and 70 kD) were used as plasma substitutes.[113] Fortunately, the dextrans used for coating magnetic particles are much lower in molecular weight (10 kD or 20 kD) and no evidence has been published to show that dextran-coated contrast agents possess side effects caused by anti-dextran antibodies.

4.2.3 Circulating behavior. The fate of the iron oxide nanoparticles is strongly dictated by their physicochemical properties, such as size, charge, hydrophilicity/hydrophobicity, and surface chemistry. A sufficiently long blood half-time is in most cases favorable for delivering the magnetic nanoparticles in deep territories and then actively targeting the pathological tissues.

The clearance of iron oxide nanoparticles intravenously injected is strongly related to the opsonization process because the nanoparticles would be firstly adsorbed by opsonins (*i.e.*, circulating plasma proteins including various subclasses of immunoglobulins, complement proteins, fibronectin, *etc.*), and then taken up by the reticuloendothelial system (RES), alternatively known as the mononuclear phagocyte system (MPS) which is defined as the cell family of bone marrow progenitors, blood monocytes and tissue macrophages (such as Kupffer cells in the liver).[114] As a result of the opsonization effect, the magnetic nanoparticles are quickly cleared from the blood compartment, as opsonins are capable of interacting with specialized plasma membrane receptors on monocytes and macrophages, thus promoting the particle recognition by these cells.[115–118] Consequently, liver, spleen and bone marrow become the most accessible tissues as they are rich in macrophages. Therefore, magnetic nanocrystals prone to be uptaken by RES can be used to better visualize these tissues by MRI. Typically, nanoparticles larger than 200 nm are sequestered by the spleen as a result of mechanical filtration and then are taken up by the phagocytic system.[119] For particles down to 100 nm or below, neutral surfaces are not sufficiently coated with the opsonizing complement proteins, and as a result are poorly recognized by Kupffer cells.[119]

The particles are endocytosed by the circulating monocytes or the tissue macrophages *via* a complex mechanism comprising phagocytosis, non-specific endocytosis, receptor-mediated endocytosis, and pinocytosis. To effectively minimize or delay the nanoparticle uptake by the RES is important for developing contrast agents with long blood half-times.

With respect to USPIO-type contrast agents, smaller particle size favors long blood circulation times for particles coated with the same materials. Apart from the particle size, the physical properties of the polymer coating materials are more important than those of the "core" material. In general, for water soluble (dispersible) nanoparticles, an ionic polymer coating leads to a higher uptake than a nonionic coating.[120] For example, cationic poly-L-lysine-coated magnetic iron oxide nanoparticles (MION-46, 21 ± 3 nm) present a half-clearance time of 1–2 min, while the uncharged counterparts presented a much longer half-clearance time of 2–3 h.[121] The short blood half-time of the positively charged particles was explained by the non-specific adsorption of particles on cells,[122] which however remains to be verified. The strong negatively charged particles also present strong liver uptake effects: for example, 8.7 nm citrate-coated iron oxide nanoparticles (VSOP) present a blood half-time of approximately 1 h in humans.[2] Therefore, to produce RES-evading nanoparticles, less-chargeable hydrophilic polymers such as linear dextran and PEG are preferred for coating the magnetic nanoparticles because they can effectively reduce protein adsorption.[111,119]

4.2.4 Elimination pathways. Bawendi *et al.* recently demonstrated that particles with hydrodynamic size smaller than 5.5 nm are rapidly removed through renal clearance. However, when the hydrodynamic size is increased to 8.6 nm, the renal clearance is significantly suppressed, leading to a long blood half-time of 20 h.[123]

For particles larger than this border size, their pathways are known as follows. Early investigations from Weissleder *et al.* demonstrate that intravenously injected iron oxide particles (AMI-25, 80 nm) undergo biodegradation and the metabolized iron (as determined by ^{59}Fe) is incorporated into hemoglobin beginning 1 to 2 days after injection, and peaking at 5–40 days.[124] At cellular level, the opsonized iron oxide particles (dextran-coated iron oxide particles with monocrystalline cores of 4.6 ± 1.2 nm) are taken up *via* receptor-mediated endocytosis rather than pinocytosis to localize to the lysosomal compartment of macrophages, and metabolized *via* the lysosomal pathway.[125] Upon the use of iron oxide particles of 5.6 ± 1.2 nm stabilized by methoxy (PEG) phosphate 2000, Briley-Saebo *et al.* investigated the retention of iron oxide particles in either Kupffer or endothelia cells by both MRI and ICP-AES (inductively coupled plasma-atomic emission spectroscopy) methods. Their investigations reveal that at 28 days post-injection, no quantifiable particles are present in either the Kupffer or endothelial cell fractions based on MRI measurements. In contrast, significant amounts of breakdown products are observed in both cell fractions based on the ICP-AES measurements. They therefore concluded that the degradation of the iron oxide particles occurs faster than the exocytosis of the breakdown products presumably as ferritin or transferrin.[126] The latter experiments might be more conclusive by taking the decrease of the contrast enhancement effect caused by the aggregation of particles into consideration. Although a large number of in vitro and in vivo experiments have been carried out on magnetic iron oxide nanoparticles, from our

point of view, their fates at cellular and sub-cellular levels must be subjected to more careful studies for elucidating the elimination pathways.

4.3 Surface functionalizability

To actively target pathological tissues, surface reactive moieties are required to further conjugate the contrast agents to targeting molecules, such as antibody, peptide, and folic acid with respect to tumor detection, for specifically recognizing the pathological cells *via* their surface receptors. To meet this requirement, surface reactive moieties such as carboxylic groups, amine groups and thiol groups are preferred as they allow further conjugation reactions with proteins or peptides to take place under mild conditions, which are important for maintaining the biological functions of targeting molecules as well as the physical properties of iron oxide nanoparticles because harsh chemical environments such as strong base, acid, or oxidative conditions will chemically destroy Fe_3O_4 nanoparticles in addition to introducing impurities. One of the most widely used conjugation reactions is l-ethyl-3-(3-dimethylaminopropyl)carbodiimide (EDC)- or EDC/N-hydroxy-succinimide (EDC-NHS)-mediated amidation reaction for chemically conjugating carboxylic group- or amine group-bearing particles to proteins or peptides. More mild conjugation reactions *via* carboxylic groups, amine groups, or thiol groups can be found from the literature.[127]

In this context, to introduce surface reactive moieties to iron oxide nanoparticle becomes the most important step for obtaining robust MRI molecular probes, because chemical bonding is quite obviously superior to physical adsorption of targeting molecules on particle surfaces. With respect to iron oxide particles prepared in aqueous systems, the surface chemistry introduced in the previous section suggests that the easiest approach would be the use of surface complexation reagents bearing excessive carboxylic groups and/or amine groups. As dextran is the most commonly used natural polymer for coating magnetic iron oxide nanoparticles, different approaches have been established for functionalizing dextran. For example, surface aldehyde groups on dextran-coated iron oxide particles can be generated upon an oxidation reaction using $NaIO_4$ or KIO_4,[128] while amine-terminated particles can be obtained by crosslinking the dextran-coated particles by epichlorohydrin and ammonia.[129]

With respect to the magnetic nanoparticles produced in non-polar solvents through thermal decomposition reactions, as they are coated by long hydrophobic chain molecules, different approaches as mentioned above have been developed for rendering them water soluble. Those approaches, in most cases, simultaneously introduce surface reactive moieties to the water-soluble particles. With respect to the phase transferring strategy, despite the overall size increase caused by the additional coating layer, the amphiphilic polymers like poly(maleic anhydride-alt-1-tetradecene) and poly(maleic anhydride-alt-1-octadecene) offer almost the ultimate solution for introducing surface reactive carboxylic groups in addition to rendering the hydrophobic particles water soluble.[106] Regarding the ligand displacement strategy, different types of surface reactive moieties can easily be introduced. For example, the displacement of surface-capped lauric acid by 2,3-dimercaptosuccinic acid gives rise to free surface thiol groups available for further bioconjugation reactions.[97] Similarly, upon the displacement of surface-bonded oleic acid by either 5-hexynoic acid or 2-azido-2-methyl-propionic acid 2-phosphonooxy-ethyl ester, alkyne or azide surface groups can be introduced and used as effective functional groups for further "click" reaction (reactions between azide and alkyne groups catalyzed by copper(I)).[130] Although "click" chemistry is still new in terms of particle surface functionalization, it may offer versatile choices.[131,132] Recently, Sun *et al.* developed another unique route for functionalizing hydrophobic particles. They adopted 4-methylcatechol (4-MC) as the surface ligand instead of oleylamine and oleic acid to produce functionalizable Fe_3O_4 nanocrystals, then the aromatic ring of 4-MC was used to directly couple the nanoparticles with amine groups from a peptide *via* a Mannich reaction.[38]

Different from all above-mentioned methods, the use of α,ω-dicarboxyl-terminated PEG as a surface capping agent enabled us to produce biocompatible Fe_3O_4 nanocrystals with surface reactive carboxylic acid groups through the thermal decomposition of $Fe(acac)_3$.[20,21] The unique feature of our synthetic route is that the preparation is carried out *via* a "one-pot" reaction. Our unpublished results further demonstrate that to use a non-polar solvent instead of 2-pyrrolidone is greatly helpful for further suppressing the size distribution of the particles bearing surface carboxylic acid groups.[133]

Certainly, surface functionalizaiton can also be achieved by coating the iron oxide particle with silica,[134] Au,[135] or polymer.[136] From the surface functionalization point of view, the silica or Au coating will offer versatile choices for coupling the particles with targeting molecules. But from the in vivo MRI application point of view, it may cause additional "trouble" in many aspects as discussed throughout this section.

5. Iron oxide-based contrast agents for disease detection

Typically, iron oxide nanoparticles are used as T2 contrast agents due to their predominant T2-relaxation effects, giving rise to signal reduction on T2-weighted images ("negative" contrast). The ability of iron oxide particles to increase the proton relaxation rates of the surrounding water proton spins is described by the relaxivity R2 (1/T2) which is associated with the magnetic susceptibility of the particles as a function of particle size and composition, in addition to experimental variables such as field strength, temperature, medium in which the relaxation times are determined (water, gels, tissue), *etc.*[137]

With respect to the in vivo applications, as the fates of the iron oxide nanoparticles are strongly governed by the particle size and surface properties, different methodologies are being established based on various biological effects and can further be classified as passive mode imaging and active mode imaging. The in vivo applications of iron oxide-based contrast agents are classified in this way because high quality iron oxide nanocrystals offered by the thermal decomposition methods possess great potential in MR molecular imaging, which is beyond what can be achieved by using iron oxide nanoparticles produced by hydrolytic synthetic methods, even though the latter type of contrast agents have been

the subject of a large number of investigations, especially at clinical levels.

5.1 Passive mode imaging

Passive mode imaging herein refers to imaging based on the natural biological distribution of iron oxide nanoparticles.

5.1.1 RES-directed MRI. Diagnoses based on RES-directed imaging have been summarized in a number of review articles.[3,11] In principle, magnetic iron oxide particles prone to be passively taken up by RES can be used for detecting diseases in tissues rich in macrophages.

Upon intravenous injection, SPIOs are easily and rapidly sequestered by macrophages in the liver and spleen, resulting in hypointensity on T2-weighted images of normal parenchyma. Since the tumor tissues are devoid of macrophages, or contain negligible or few RES cells in comparison with normal tissue, the tumors are visualized with increased conspicuousness and vice versa for focal nodular hyperplasia due to its higher content of RES cells.[138] SPIO particles are typical liver contrast agents, for example, AMI-25 developed by Advanced Magnetics accumulates in liver by approximately 80% and in spleen by 5–10% of the injected dose in humans,[139] thus presenting a very short blood half-time of 6 min.[35] By an injection dose of 20 μmol Fe/kg, the signal intensity of normal human liver decreases by 66% (SE 1500/40/2).[140] In one clinical study, the tumor/liver contrast-to-noise ratio (CNR) was observed to increase from 0.6 ± 4.9 to 16.3 ± 9.6 on T2-weighted images and hepatic tumor deposits as small as 3 mm were detected.[140,141] In another study performed on spleen, 45 lesions were visible on enhanced MRI contrasting to 4 on un-enhanced MRI.[142]

USPIOs with smaller size and longer blood half-time are enabled to cross the capillary wall and have more widespread tissue distribution, leading to extensive uptake by the RES cells of lymph nodes and bone marrow.[3] The delivery of nanoparticles to lymph nodes is realized probably by two different pathways: 1) by direct transcapillary passage through endothelial venules into the medullary sinuses of the lymph node, followed by macrophage phagocytosis; 2) *via* non-selective endothelial transcytosis into the interstitial space in the body, followed by uptake of the nanoparticles by draining lymphatic vessels and transport to lymph nodes.[35,143] Normal functioning lymph nodes contain macrophages and present reduced signals upon uptake of USPIOs, while the metastatic nodes that are partially or completely replaced by tumor cells do not possess the same levels of phagocytotic activity as normal nodes, and thus maintain the same T2 signal intensity in the post-contrast images.[2,143] By this method, very small metastases of less than 2 mm are identified within normal-sized lymph nodes. Similarly, USPIO can be used to differentiate abnormal marrow from normal marrow based on the altered phagocytic activity of the local RES cells.[144]

MRI detection of other diseases associated with phagocytes in inflammatory and degenerative diseases, such as stroke, atherosclerosis, multiple sclerosis, kidney disease, oscteoarticular, infection and cardiac graft rejection, has also been reported by using RES-directed USPIOs.[2] The contrast enhancement effects are attributed either to local macrophage uptake after transcytosis of these nanoparticles through the endothelium or to the infiltration of activated blood monocytes which have already taken up USPIOs.[145,146]

5.1.2 Blood pool imaging. Blood pool imaging requires the contrast agents to remain in the blood for sufficient time for data acquisition during radiological procedures and show low interstitial background enhancement. The mammalian vasculature has an average pore size of ~5 nm. Particles larger than the pore size may present prolonged blood half-time and reduced renal clearance upon proper surface modification.[123] USPIOs such as Feruomoxtran-10, SHU 555C, Feruglose and VSOP-C184 have been evaluated in MR angiography (MRA) for different territories, such as coronary, pulmonary, or peripheral angiography.[147–158]

5.1.3 Tissue perfusion imaging. Iron oxide nanoparticles with long blood half-time are also very suitable as perfusion imaging agents due to their much bigger size in comparison with small molecular imaging agents. Microvascular hyperpermeability happening in neoplasms, inflammation, infection and ischemia provides the possibility for USPIOs to be used as detection agents.[3] For example, by the enhanced permeability and retention (EPR) effect of tumors, USPIO are used for tumor detection.[159,160] We also use PEG-coated Fe_3O_4 nanoparticles in detecting toxoplasmic lesions in mouse brain. The toxoplasmic lesions are clearly visible in post-contrast T2*-images as shown in

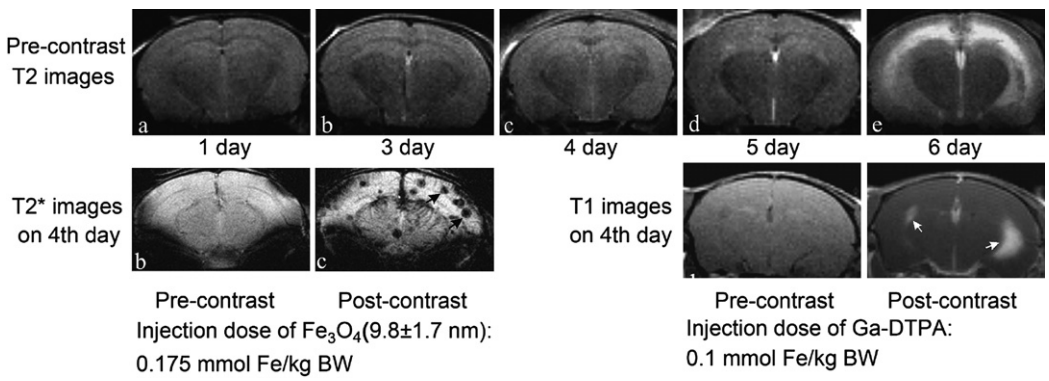

Fig. 5 Upper row: T2-weighted MR images (TR/TE = 2500/75 ms) of coronal brain slices of mice infected with *T. gondii* acquired on different days after infection; lower row: MR images acquired on the fourth day after infection. The two groups of images in the lower row were recorded before and after intravenous injections of Fe_3O_4 (left) and Ga-DTPA (right), respectively. (Reprinted from ref. 75 with permission.)

Fig. 5, which reflect blood-brain barrier impairment and/or inflammatory reactions associated with these lesions.[75]

5.2 Active mode imaging

MR active mode imaging for detecting diseases such as early tumors has provoked great research interest over the past several years.[21,37,38,98,161–174] It refers to MR imaging realized by the contrast agents which are capable of actively targeting specific diseased sites upon various molecular recognition events, leading to the emergence of MR molecular imaging. The target-specific deliveries of nanoparticles used in active mode imaging can roughly be classified into two groups. The first group of approaches adopts targeting molecules such as protein,[21,37,98,161–164] peptide,[38,165–170,174] folic acid,[171,172] *etc.*, which are in most cases covalently bonded to iron oxide particles, while the second group of approaches takes T-lymphocyte as vehicles and target disease sites *via* the cell surface expressed antigen-specific antibody.[173]

5.2.1 Targeting molecule-mediated imaging. To prepare molecular probes based on iron oxide nanoparticles, the following two prerequisites must be fulfilled, *i.e.*, RES-evading properties of the particles and the preservation of the bioactivity of targeting molecules through coupling reactions.

Early pioneering work was carried out by simple adsorption of antibodies on magnetic nanoparticles.[175] By covalently conjugating monoclone antibody to iron oxide nanoparticles, Weissleder *et al.* developed magnetic iron oxide particle-antibody probes and used them in tumor detection in vivo. Although the specificity of the probes is not very evident, these investigations pioneered the MR molecular imaging of tumors.[163]

Benefiting from the high quality of the magnetic nanocrystals prepared by the thermal decomposition method and various approaches established for particle surface functionalization, the new generation of MR molecular imaging probes exert greatly improved efficacies for targeting tumors in vivo for early tumor detection and even differentiation. Cheon *et al.* reported the in vivo imaging of breast cancer using the Fe_3O_4-herceptin probe. Herceptin as a specific antibody can target breast cancer cells overexpressing HER2/neu (epidermal growth factor receptor 2).[98] Significantly improved molecular imaging of cancers is realized by using $MnFe_2O_4$ nanocrystals instead of Fe_3O_4 nanocrystals as they possess much higher mass magnetization value than the latter ones (110 *vs.* 80 emu/g magnetic atoms). Effective R2 increases, *i.e.*, ~25% (1 h) and ~34% (2 h), much higher than the values achieved using CLIO (~5%; CLIO: ~45 nm crosslinked aminated dextran particles incorporated with 5 nm iron oxide nanocrystals), are observed from post-injection T2-weighted MR images which are acquired with a 1.5 T clinical MRI instrument with a micro surface coil. By using a $MnFe_2O_4$-herceptin probe, tumors as small as ~ 50 mg can be detected.[37]

The "one-pot" thermal decomposition method we developed offers a facile approach for preparing Fe_3O_4 nanocrystals with surface reactive carboxylic groups.[20] By EDC/NHS-mediated amidation reaction, anti-carcinoembryonic antigen (CEA) monoclonal antibody rch 24 (rch 24 mAb) is conjugated to the PEG-coated Fe_3O_4 nanocrystals, forming a MR molecular imaging probe. Both in vitro and in vivo experiments suggest that the resultant probe can specifically target human colon carcinoma cells and xenograft implanted in nude mice, as shown in Fig. 6.[21] Different from Cheon's investigations, the T2 decrease reaches a maximum at 24 h post-injection, but only by 10%. Our unpublished results further suggest that a much improved tumor specificity can be obtained by using PEG-coated Fe_3O_4 prepared by a modified recipe. Under optimized conditions, a R2 increase up to 45% can be achieved at 24 h post-injection using a 3 T clinical MRI instrument equipped with an animal coil developed by GE HealthCare, China.[133]

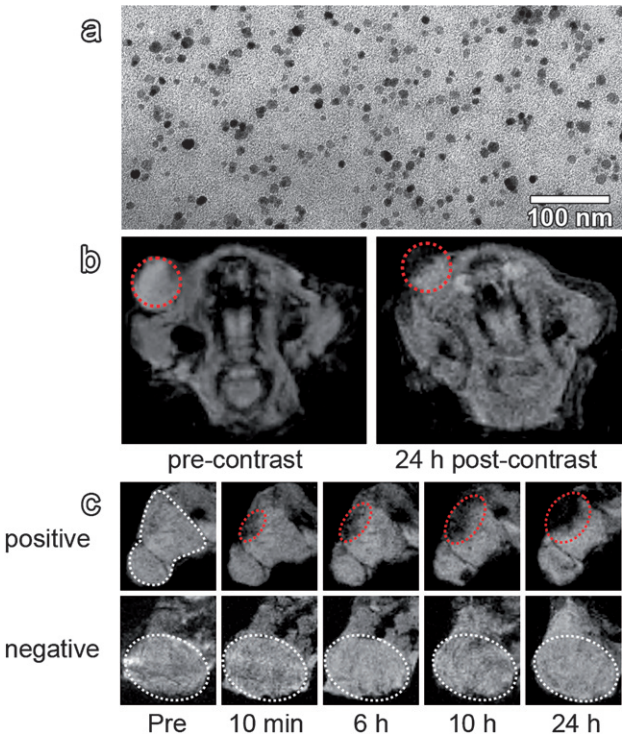

Fig. 6 a) TEM image of as-prepared PEG-coated Fe_3O_4 nanocrystals with surface reactive carboxylic groups (Fe_3O_4@PEG-COOH). b) T2*-weighted MR images acquired before and after the injection of Fe_3O_4-(rch 24 mAb) conjugates. c) T2*-weighted MR images of two tumors acquired before and at different times after intravenous injections of Fe_3O_4-(rch 24 mAb) conjugates (upper row) and Fe_3O_4@PEG-COOH nanocrystals (lower row), respectively. (Reprinted from ref. 21 with permission.)

Although antibody is a good choice for tumor targeting, the conjugate of nanoparticles and antibody inevitably suffers from its large hydrodynamic size and diffuses poorly through biological barriers and may also lead to easy uptake by RES.[176,177] Thus, small targeting molecules become alternative choices. Integrins are ubiquitous membrane proteins. Certain integrins, such as $\alpha_v\beta_3$, are upregulated on tumor cells in comparison with healthy tissue.[178] Therefore, it is a useful target for tumor detections. Since a specific tripeptide sequence, *i.e.*, arginine-glycine-aspartic acid (RGD), can specifically bind to $\alpha_v\beta_3$, it is often used to couple with iron oxide nanoparticles in detecting tumors including breast tumors, malignant melanomas, and squamous cell carcinomas.[38,67,69,179] Because RGD peptide and derivatives are much smaller than iron oxide particles, increasing the number of RGD molecules bonded per particle can increase the binding efficacy of iron oxide particles to target cells due to

a multivalent binding effect.[167] Other functional peptide such as chlorotoxin (CTX, a 36 amino acid peptide) can simultaneously be used for both MR molecular imaging and tumor therapeutic purpose.[170]

Apart from peptides, folic acid (FA) as a small tumor-targeting molecule can be recognized by folate receptors overexpressed on the surface of many human tumor cells, including ovarian, lung, breast, endometrial, renal, and colon cancers, *etc*.[180,181] Moreover, the internalization of particles conjugated to folic acid (FA) can be facilitated *via* folate receptor-mediated endocytosis.[171,182] In vitro cellular targeting experiments suggest that a Fe_3O_4-FA conjugate can specifically bind to tumor cells.[171] In vivo tumor detection experiments using a SPIO-PEG-FA contrast agent on human nasopharyngeal epidermal carcinoma cells (KB cells) reveal a signal intensity change in positive KB cell tumors by −20 to −25%, extracted from the pre-contrast and post-contrast images.[172] Another advantage of peptide and folic acid over antibody is that they allow more chemical reactions to be used for constructing the molecular probes due to their better tolerance of organic solvents and harsh chemical environments.

5.2.2 T-Lymphocyte-mediated imaging. Immune cells such as T-lymphocytes are receiving more attention due to their antigen-specific cytotoxicity which is being used for cell-based therapies of cancer[183,184] and inflammatory diseases.[185] They therefore can potentially be used as vehicles for delivering iron oxide nanoparticles to the diseased sites.[173] In this context, effective loading of magnetic iron oxide particles is important. In fact, several parameters affect the internalization of iron oxide nanoparticles into cells, such as size, surface charge, and surface chemical composition. In general, positively charged surfaces favor particle internalization.[121,186] Transfection agents can also promote the particle internalization: for example, Weissleder *et al.*[173] reported HIV Tat peptide derivatized magnetic nanoparticles with enhanced cell internalization ability for in vivo high resolution three-dimensional MR imaging of antigen-specific cytotoxic T-lymphocyte trafficking to tumors. Apart from the loading efficiency, to effectively prevent the loaded particles from aggregating within cells is also important, especially for in vivo monitoring of stem cells[186] or progenitor cells migration.[187] As a matter of fact, cell magnetic labeling has many other potential applications beyond tumor detection,[2] which will not be discussed here due to the limitation of space.

6. Remarks and perspectives

Superparamagnetic iron oxide nanoparticles have received great attention over the past 3 decades due to their application in MRI as contrast agents. Recent developments in the syntheses of high quality magnetic nanoparticles have however introduced new blood into this interdisciplinary field.

Until now, commercial iron oxide-based contrast agents are exclusively produced by hydrolytic synthetic routes, *e.g.*, the coprecipitation method. The growth of iron oxide nanoparticles in aqueous media is heavily controlled by a large number of kinetic factors not only because water and hydroxyl ions are involved, but also because complicated surface dynamics are induced by the strong polar aqueous media. Thus the resultant iron oxide particles are generally characterized by wide particle size distributions and relatively low magnetic susceptibility. In contrast, the recently developed thermal decomposition method overcomes the intrinsic drawbacks by adopting a different synthetic principle, *i.e.*, pyrolysis rather than hydrolysis. Consequently the number of kinetic factors for growing iron oxide particles is greatly reduced in the high temperature environment due to the absence of bulk water and the indissolubility of iron oxides in non-polar and weak polar solvents. Thus, uniform iron oxide nanocrystals become more facilely available through the thermal decomposition method as the surface dynamics are greatly simplified in comparison with those occurring in aqueous systems.

Nevertheless, acids, alcohols, and amines bearing long hydrophobic chains are required to produce iron oxide nanocrystals to eventually provide them with surfaces compatible with non-polar environments. Consequently the direct products of the thermal decomposition syntheses are typically characterized by hydrophobicity. Only through further surface engineering by taking the surface biocompatibility and functionalizability into consideration do they become usable as MRI contrast agents. We developed an alternative approach to achieve water soluble and biocompatible iron oxide nanocrystals while inheriting the advantages of the thermal decomposition method by replacing the non-polar or weak polar solvents with strong polar solvents, which further allowed us to effectively combine the particle synthetic chemistry with surface engineering chemistry, consequently different types of biocompatible Fe_3O_4 nanocrystals can be obtained *via* "one-pot" reactions, which greatly simplifies the procedures for producing high quality MRI contrast agents.

Even though the commercial iron oxide-based contrast agents were largely evaluated at preclinical and clinical stages more than 10 years ago, the perfect particle size monodispersity, tunability, satisfactory magnetic susceptibility due to the higher phase purity of magnetic iron oxide particles offered by the thermal decomposition method, together with various techniques available for more delicate surface engineering provide new generations of contrast agents by which more details of various biological and biomedical events may be hopefully revealed. In this context, some of the conclusions based on the commercial contrast agents may need to be reconsidered.

To target specific pathological sites in vivo *via* particle surface coupled targeting molecules has become an important trend, leading to new conceptual MR molecular imaging. The great advantage of using iron oxide nanoparticles to construct molecular probes is that the particles offer multiple surface binding sites by which various types of biological probes can be simultaneously attached, giving rise to multi-functional probes combining different imaging modes[133,188] or both imaging and therapeutics.

The precise particle size control achieved by the thermal decomposition method provides great opportunities to reveal the particle size-dependent behavior in a more reliable way, such as the particle size-dependent fate and permeability across various biological barriers.[189] Towards these investigations, clearly defining the surface structures of differently sized nanoparticles remains challenging.

In summary, great advancements in the syntheses of high quality magnetic iron oxide nanocrystals are providing new possibilities for improving the efficiency and efficacy of medical

diagnosis based on superparamagnetic iron oxide nanoparticle-enhanced MRI. In this multidisciplinary field, discovering, developing and understanding the underlying chemistry for particle size and surface control are of the utmost importance.

Acknowledgements

The current investigations are jointly supported by NSFC projects (20820102035, 20673128, 20773140, 20640430564) and an 863 project (2007AA02Z467).

References

1 V. Wagner, A. Dullaart, A. K. Bock and A. Zweck, *Nat. Biotechnol.*, 2006, **24**, 1211.
2 C. Corot, P. Robert, J. M. Idee and M. Port, *Adv. Drug Del. Rev.*, 2006, **58**, 1471.
3 Y. X. J. Wang, S. M. Hussain and G. P. Krestin, *Eur. Radiol.*, 2001, **11**, 2319.
4 J. Park, J. Joo, S. G. Kwon, Y. Jang and T. Hyeon, *Angew. Chem. Int. Ed. Engl.*, 2007, **46**, 4630.
5 S. Laurent, D. Forge, M. Port, A. Roch, C. Robic, L. V. Elst and R. N. Muller, *Chem. Rev.*, 2008, **108**, 2064.
6 M. A. Willard, L. K. Kurihara, E. E. Carpenter, S. Calvin and V. G. Harris, *Int. Mater. Rev.*, 2004, **49**, 125.
7 A. H. Lu, E. L. Salabas and F. Schuth, *Angew. Chem. Int. Ed. Engl.*, 2007, **46**, 1222.
8 Y. W. Jun, J. H. Lee and J. W. Cheon, *Angew. Chem. Int. Ed. Engl.*, 2008, **47**, 5122.
9 A. K. Gupta and M. Gupta, *Biomaterials*, 2005, **26**, 3995.
10 C. Sun, J. S. H. Lee and M. Q. Zhang, *Adv. Drug Del. Rev.*, 2008, **60**, 1252.
11 A. K. Gupta, R. R. Naregalkar, V. D. Vaidya and M. Gupta, *Nanomedicine*, 2007, **2**, 23.
12 J. Rockenberger, E. C. Scher and A. P. Alivisatos, *J. Am. Chem. Soc.*, 1999, **121**, 11595.
13 T. Hyeon, S. S. Lee, J. Park, Y. Chung and H. Bin Na, *J. Am. Chem. Soc.*, 2001, **123**, 12798.
14 T. Hyeon, *Chem. Commun.*, 2003, 927.
15 J. Park, K. J. An, Y. S. Hwang, J. G. Park, H. J. Noh, J. Y. Kim, J. H. Park, N. M. Hwang and T. Hyeon, *Nat. Mater.*, 2004, **3**, 891.
16 S. H. Sun and H. Zeng, *J. Am. Chem. Soc.*, 2002, **124**, 8204.
17 S. H. Sun, H. Zeng, D. B. Robinson, S. Raoux, P. M. Rice, S. X. Wang and G. X. Li, *J. Am. Chem. Soc.*, 2004, **126**, 273.
18 N. R. Jana, Y. Chen and X. G. Peng, *Chem. Mater.*, 2004, **16**, 3931.
19 J. W. Cheon, N. J. Kang, S. M. Lee, J. H. Lee, J. H. Yoon and S. J. Oh, *J. Am. Chem. Soc.*, 2004, **126**, 1950.
20 F. Q. Hu, Z. Li, C. F. Tu and M. Y. Gao, *J. Colloid Interface Sci.*, 2007, **311**, 469.
21 F. Q. Hu, L. Wei, Z. Zhou, Y. L. Ran, Z. Li and M. Y. Gao, *Adv. Mater.*, 2006, **18**, 2553.
22 Z. Li, L. Wei, M. Y. Gao and H. Lei, *Adv. Mater.*, 2005, **17**, 1001.
23 Z. Li, H. Chen, H. B. Bao and M. Y. Gao, *Chem. Mater.*, 2004, **16**, 1391.
24 Z. Li, Q. Sun and M. Y. Gao, *Angew. Chem. Int. Ed. Engl.*, 2005, **44**, 123.
25 X. Y. Lu, M. Niu, R. R. Qiao and M. Y. Gao, *J. Phys. Chem. B*, 2008, **112**, 14390.
26 P. C. Lauterbur, *Nature*, 1973, **242**, 190.
27 K. M. Mudry, R. Plonsey and J. Bronzino, *Biomedical imaging*, CRC Press, Boca Raton, 2003.
28 W. F. Brown, *Phys. Rev.*, 1963, **1**, 1677.
29 D. Jiles, *Introduction to Magnetism and Magnetic Materials*, Chapman and Hall, London, 1991.
30 A. H. Morrish, *The Physical Principles of Magnetism*, IEEE Press, New York:, 2001.
31 Q. A. Pankhurst, J. Connolly, S. K. Jones and J. Dobson, *J. Phys. D-Appl. Phys.*, 2003, **36**, R167.
32 G. L. Wolf and E. S. Fobben, *Invest. Radiol.*, 1984, **19**, 324.
33 H. J. Weinmann, R. C. Brasch, W. R. Press and G. E. Wesbey, *Am. J. Roentgenol.*, 1984, **142**, 619.
34 Y. W. Jun, J. W. Seo and J. W. Cheon, *Acc. Chem. Res.*, 2008, **41**, 179.
35 R. Weissleder, G. Elizondo, J. Wittenberg, C. A. Rabito, H. H. Bengele and L. Josephson, *Radiology*, 1990, **175**, 489.
36 M. G. Harisinghani, J. Barentsz, P. F. Hahn, W. M. Deserno, S. Tabatabaei, C. H. van de Kaa, J. de la Rosette and R. Weissleder, *New Engl. J. Med.*, 2003, **348**, 2491.
37 J. H. Lee, Y. M. Huh, Y. Jun, J. Seo, J. Jang, H. T. Song, S. Kim, E. J. Cho, H. G. Yoon, J. S. Suh and J. W. Cheon, *Nat. Med.*, 2007, **13**, 95.
38 J. Xie, K. Chen, H. Y. Lee, C. J. Xu, A. R. Hsu, S. Peng, X. Y. Chen and S. H. Sun, *J. Am. Chem. Soc.*, 2008, **130**, 7542.
39 D. J. Dunlop, *Journal of Geophysical Research*, 1973, **78**, 1780.
40 G. Bate, in *Ferromagnetic Materials*, ed. E. P. Wohlfarth, Elsevier, North Holland, 1980, vol. 2, pp. 439.
41 U. Schwertmann and R. M. Cornell, *Iron Oxides in the Laboratory*, Wiley-VCH, Weinheim, 2000.
42 L. A. Welo and O. Baudisch, *Philos. Mag.*, 1925, **50**, 399.
43 I. David and A. J. E. Welch, *Trans. Faraday Soc.*, 1956, **52**, 1642.
44 S. C. Qu, H. B. Yang, D. W. Ren, S. H. Kan, G. T. Zou, D. M. Li and M. H. Li, *J. Colloid Interface Sci.*, 1999, **215**, 190.
45 Y. S. Kang, S. Risbud, J. F. Rabolt and P. Stroeve, *Chem. Mater.*, 1996, **8**, 2209.
46 A. Bee, R. Massart and S. Neveu, *J. Magn. Magn. Mater.*, 1995, **149**, 6.
47 W. C. Elmore, *Phys. Rev.*, 1938, **54**, 309.
48 C. R. Ricketts, J. S. G. Cox, C. Fitzmaur and G. F. Moss, *Nature*, 1965, **208**, 237.
49 B. H. Gu, T. L. Mehlhorn, L. Y. Liang and J. F. McCarthy, *Geochim. Cosmochim. Acta*, 1996, **60**, 1943.
50 F. Sauzedde, A. Elaissari and C. Pichot, *Colloid. Polym. Sci.*, 1999, **277**, 846.
51 E. K. Kim and H. W. Walker, *Colloid Surf. A-Physicochem. Eng. Asp*, 2001, **194**, 123.
52 E. Tombacz, E. Illes, A. Majzik, A. Hajdu, N. Rideg and M. Szekeres, *Croat. Chem. Acta*, 2007, **80**, 503.
53 Z. X. Sun, F. W. Su, W. Forsling and P. O. Samskog, *J. Colloid Interface Sci.*, 1998, **197**, 151.
54 B. H. Gu, J. Schmitt, Z. H. Chen, L. Y. Liang and J. F. Mccarthy, *Environ. Sci. Technol.*, 1994, **28**, 38.
55 B. H. Gu, J. Schmitt, Z. Chen, L. Y. Liang and J. F. Mccarthy, *Geochim. Cosmochim. Acta*, 1995, **59**, 219.
56 Q. Wang, Y. C. Kuo, Y. W. Wang, G. Shin, C. Ruengruglikit and Q. R. Huang, *J. Phys. Chem. B*, 2006, **110**, 16860.
57 T. Ishikawa, S. Kataoka and K. Kandori, *J. Mater. Sci.*, 1993, **28**, 2693.
58 W. J. Lee and T. T. Fang, *J. Mater. Sci.*, 1995, **30**, 4349.
59 N. Fauconnier, A. Bee, J. Roger and J. N. Pons, *Prog. Colloid Polym. Sci.*, 1996, **100**, 212.
60 Y. Sahoo, H. Pizem, T. Fried, D. Golodnitsky, L. Burstein, C. N. Sukenik and G. Markovich, *Langmuir*, 2001, **17**, 7907.
61 P. Persson, N. Nilsson and S. Sjoberg, *J. Colloid Interface Sci.*, 1996, **177**, 263.
62 C. Liu and P. M. Huang, *Soil Sci. Soc. Am. J.*, 1999, **63**, 65.
63 R. Massart, *IEEE Trans. Magn.*, 1981, **17**, 1247.
64 R. Massart and V. Cabuil, *J. Chim. Phys. Phys.- Chim. Biol.*, 1987, **84**, 967.
65 R. Massart, *Cr Acad Sci C Chim*, 1980, **291**, 1.
66 R. Massart, E. Dubois, V. Cabuil and E. Hasmonay, *J. Magn. Magn. Mater.*, 1995, **149**, 1.
67 N. Munshi, T. K. De and A. Maitra, *J. Colloid Interface Sci.*, 1997, **190**, 387.
68 X. Wang, J. Zhuang, Q. Peng and Y. D. Li, *Nature*, 2005, **437**, 121.
69 J. Xu, H. B. Yang, W. Y. Fu, K. Du, Y. M. Sui, J. J. Chen, Y. Zeng, M. H. Li and G. Zou, *J. Magn. Magn. Mater.*, 2007, **309**, 307.
70 C. Pascal, J. L. Pascal, F. Favier, M. L. E. Moubtassim and C. Payen, *Chem. Mater.*, 1999, **11**, 141.
71 R. Abu Mukh-Qasem and A. Gedanken, *J. Colloid Interface Sci.*, 2005, **284**, 489.
72 X. Cao, Y. Koltypin, R. Prozorov and G. Kataby, *J. Mater. Chem.*, 1997, **7**, 2447.
73 K. Woo, J. Hong, S. Choi, H. W. Lee, J. P. Ahn, C. S. Kim and S. W. Lee, *Chem. Mater.*, 2004, **16**, 2814.
74 W. W. Yu, J. C. Falkner, C. T. Yavuz and V. L. Colvin, *Chem. Commun.*, 2004, 2306.

75 L. Wei, G. Zhou, Z. Li, L. He, M. Y. Gao, J. Q. Tan and H. Lei, *Magn. Reson. Imaging*, 2007, **25**, 1442.
76 V. K. LaMer and R. H. Dinegar, *J. Am. Chem. Soc.*, 1950, **72**, 4847.
77 C. B. Murray, D. J. Norris and M. G. Bawendi, *J. Am. Chem. Soc.*, 1993, **115**, 8706.
78 X. G. Peng, J. Wickham and A. P. Alivisatos, *J. Am. Chem. Soc.*, 1998, **120**, 5343.
79 Y. F. Chen, E. Johnson and X. G. Peng, *J. Am. Chem. Soc.*, 2007, **129**, 10937.
80 X. G. Peng and J. Thessing, *Semiconductor Nanocrystals and Silicate Naoparticles*, Springer, Berlin, 2005, pp. 79.
81 Y. Yin and A. P. Alivisatos, *Nature*, 2005, **437**, 664.
82 G. Schmid, N. Klein, B. Morun and A. Lehnert, *Pure Appl. Chem.*, 1990, **62**, 1175.
83 M. M. Alvarez, J. T. Khoury, T. G. Schaaff, M. Shafigullin, I. Vezmar and R. L. Whetten, *Chem. Phys. Lett.*, 1997, **266**, 91.
84 M. N. Vargaftik, V. P. Zagorodnikov, I. P. Stolarov, I. I. Moiseev, D. I. Kochubey, V. A. Likholobov, A. L. Chuvilin and K. I. Zamaraev, *J. Mol. Catal.*, 1989, **53**, 315.
85 M. A. Watzky and R. G. Finke, *J. Am. Chem. Soc.*, 1997, **119**, 10382.
86 I. L. Garzon, K. Michaelian, M. R. Beltran, A. Posada-Amarillas, P. Ordejon, E. Artacho, D. Sanchez-Portal and J. M. Soler, *Phys. Rev. Lett.*, 1998, **81**, 1600.
87 T. Vossmeyer, G. Reck, L. Katsikas, E. T. K. Haupt, B. Schulz and H. Weller, *Science*, 1995, **267**, 1476.
88 S. Behrens, M. Bettenhausen, A. C. Deveson, A. Eichhofer, D. Fenske, A. Lohde and U. Woggon, *Angew. Chem. Int. Ed. Engl.*, 1996, **35**, 2215.
89 N. V. Soloviev, A. Eichhofer, D. Fenske and U. Banin, *J. Am. Chem. Soc.*, 2001, **123**, 2354.
90 C. F. Tu, J. J. Du, L. Yao, C. H. Yang, M. F. Ge, C. L. Xu and M. Y. Gao, *J. Mater. Chem.*, 2009, **19**, 1245.
91 N. Pradhan, D. Reifsnyder, R. G. Xie, J. Aldana and X. G. Peng, *J. Am. Chem. Soc.*, 2007, **129**, 9500.
92 K. Byrappa, S. Ohara and T. Adschiri, *Adv. Drug Del. Rev.*, 2008, **60**, 299.
93 Y. Wang, S. Maksimuk, R. Shen and H. Yang, *Green Chem.*, 2007, **9**, 1051.
94 A. M. E. Tombácz, Z. S. Horvát and E. illés, *Rom. Rep. Phys.*, 2006, **58**, 281.
95 S. Mohapatra, N. Pramanik, S. K. Ghosh and P. Pramanik, *J. Nanosci. Nanotechnol.*, 2006, **6**, 823.
96 H. Lee, E. Lee, D. K. Kim, N. K. Jang, Y. Y. Jeong and S. Jon, *J. Am. Chem. Soc.*, 2006, **128**, 7383.
97 Y. W. Jun, Y. M. Huh, J. S. Choi, J. H. Lee, H. T. Song, S. Kim, S. Yoon, K. S. Kim, J. S. Shin, J. S. Suh and J. W. Cheon, *J. Am. Chem. Soc.*, 2005, **127**, 5732.
98 Y. M. Huh, Y. W. Jun, H. T. Song, S. Kim, J. S. Choi, J. H. Lee, S. Yoon, K. S. Kim, J. S. Shin, J. S. Suh and J. W. Cheon, *J. Am. Chem. Soc.*, 2005, **127**, 12387.
99 H. W. Gu, K. M. Xu, Z. M. Yang, C. K. Chang and B. Xu, *Chem. Commun.*, 2005, 4270.
100 S. Peng, C. Wang, J. Xie and S. H. Sun, *J. Am. Chem. Soc.*, 2006, **128**, 10676.
101 C. Xu, K. Xu, H. Gu, R. Zheng, H. Liu, X. Zhang, Z. Guo and B. Xu, *J. Am. Chem. Soc.*, 2004, **126**, 9938.
102 R. Hong, N. O. Fischer, T. Emrick and V. M. Rotello, *Chem. Mater.*, 2005, **17**, 4617.
103 J. H. Choy, Y. S. Han and S. W. Song, *Mater. Lett.*, 1994, **19**, 257.
104 D. B. Robinson, H. H. J. Persson, H. Zeng, G. X. Li, N. Pourmand, S. H. Sun and S. X. Wang, *Langmuir*, 2005, **21**, 3096.
105 N. Nitin, L. E. W. LaConte, O. Zurkiya, X. Hu and G. Bao, *J. Biol. Inorg. Chem.*, 2004, **9**, 706.
106 T. Pellegrino, L. Manna, S. Kudera, T. Liedl, D. Koktysh, A. L. Rogach, S. Keller, J. Radler, G. Natile and W. J. Parak, *Nano Lett.*, 2004, **4**, 703.
107 W. W. Yu, E. Chang, C. M. Sayes, R. Drezek and V. L. Colvin, *Nanotechnology*, 2006, **17**, 4483.
108 D. F. Williams, *Biomaterials*, 2008, **29**, 2941.
109 M. L. Bassett, J. W. Halliday and L. W. Powell, *Hepatology*, 1986, **6**, 24.
110 A. S. Tavill and B. R. Bacon, *Hepatology*, 1986, **6**, 142.
111 S. Mornet, S. Vasseur, F. Grasset and E. Duguet, *J. Mater. Chem.*, 2004, **14**, 2161.
112 A. Stroh, C. Zimmer, C. Gutzeit, M. Jakstadt, F. Marschinke, T. Jung, H. Pilgrimm and T. Grune, *Free Radical Biol. Med.*, 2004, **36**, 976.
113 C. E. Zinderman, L. Landow and R. P. Wise, *J. Vasc. Surg.*, 2006, **43**, 1004.
114 D. A. Hume, I. L. Ross, S. R. Himes, R. T. Sasmono, C. A. Wells and T. Ravasi, *J. Leukocyte Biol.*, 2002, **72**, 621.
115 A. Chonn, S. C. Semple and P. R. Cullis, *J. Biol. Chem.*, 1992, **267**, 18759.
116 S. M. Moghimi and S. S. Davis, *Crit. Rev. Ther. Drug Carr. Syst.*, 1994, **11**, 31.
117 S. M. Moghimi and H. M. Patel, *Adv. Drug Del. Rev.*, 1998, **32**, 45.
118 S. M. Moghimi and A. C. Hunter, *Pharm. Res.*, 2001, **18**, 1.
119 S. M. Moghimi, A. C. Hunter and J. C. Murray, *Pharmacol. Rev.*, 2001, **53**, 283.
120 S. Metz, S. Lohr, M. Settles, A. Beer, K. Woertler, E. Rummeny and H. E. Daldrup-Link, *Eur. Radiol.*, 2006, **16**, 598.
121 M. I. Papisov, A. Bogdanov Jr, B. Schaffer, N. Nossiff, T. Shen, R. Weissleder and T. J. Brady, *J. Magn. Magn. Mater.*, 1993, **122**, 383.
122 T. Fujita, M. Nishikawa, Y. Ohtsubo, J. Ohno, Y. Takakura, H. Sezaki and M. Hashida, *J. Drug Target.*, 1994, **2**, 157.
123 H. S. Choi, W. Liu, P. Misra, E. Tanaka, J. P. Zimmer, B. I. Ipe, M. G. Bawendi and J. V. Frangioni, *Nat. Biotechnol.*, 2007, **25**, 1165.
124 R. Weissleder, D. D. Stark, B. L. Engelstad, B. R. Bacon, C. C. Compton, D. L. White, P. Jacobs and J. Lewis, *Am. J. Roentgenol.*, 1989, **152**, 167.
125 E. Schulze, J. T. Ferrucci, K. Poss, L. Lapointe, A. Bogdanova and R. Weissleder, *Invest. Radiol.*, 1995, **30**, 604.
126 K. Briley-Saebo, A. Bjornerud, D. Grant, H. Ahlstrom, T. Berg and G. M. Kindberg, *Cell Tissue Res.*, 2004, **316**, 315.
127 G. T. Hermanson, *Bioconjugate Techniques*, Elsevier, Amsterdam, 2nd edn, 2008.
128 R. S. Molday and D. Mackenzie, *J. Immunol. Methods*, 1982, **52**, 353.
129 P. Wunderbaldinger, L. Josephson and R. Weissleder, *Bioconjugate Chem.*, 2002, **13**, 264.
130 M. A. White, J. A. Johnson, J. T. Koberstein and N. J. Turro, *J. Am. Chem. Soc.*, 2006, **128**, 11356.
131 K. El-Boubbou, C. Gruden and X. Huang, *J. Am. Chem. Soc.*, 2007, **129**, 13392.
132 L. Polito, D. Monti, E. Caneva, E. Delnevo, G. Russo and D. Prosperi, *Chem. Commun.*, 2008, 621.
133 S. J. Liu, B. Jia, R. R. Qiao, Z. Yang, Z. L. Yu, Z. H. Liu, K. Liu, H. Ouyang, F. Wang and M. Y. Gao, *Molecular Pharmaceutics*, in revision.
134 C. W. Lai, Y. H. Wang, C. H. Lai, M. J. Yang, C. Y. Chen, P. T. Chou, C. S. Chan, Y. Chi, Y. C. Chen and J. K. Hsiao, *Small*, 2008, **4**, 218.
135 S. J. Cho, B. R. Jarrett, A. Y. Louie and S. M. Kauzlarich, *Nanotechnology*, 2006, **17**, 640.
136 Y. Wang, X. W. Teng, J. S. Wang and H. Yang, *Nano Lett.*, 2003, **3**, 789.
137 A. Bogdanov, R. Weissleder and T. J. Brady, *Adv. Drug Del. Rev.*, 1995, **16**, 335.
138 R. C. Semelka and T. K. G. Helmberger, *Radiology*, 2001, **218**, 27.
139 P. Reimer and B. Tombach, *Eur. Radiol.*, 1998, **8**, 1198.
140 D. D. Stark, R. Weissleder, G. Elizondo, P. F. Hahn, S. Saini, L. E. Todd, J. Wittenberg and J. T. Ferrucci, *Radiology*, 1988, **168**, 297.
141 C. Chambon, O. Clement, A. Leblanche, E. Schoumanclaeys and G. Frija, *Magn. Reson. Imaging*, 1993, **11**, 509.
142 R. Weissleder, P. F. Hahn, D. D. Stark, G. Elizondo, S. Saini, L. E. Todd, J. Wittenberg and J. T. Ferrucci, *Radiology*, 1988, **169**, 399.
143 M. F. Bellin, C. Beigelman and S. Precetti-Morel, *Eur. J. Radiol.*, 2000, **34**, 257.
144 E. Seneterre, R. Weissleder, D. Jaramillo, P. Reimer, A. S. Lee, T. J. Brady and J. Wittenberg, *Radiology*, 1991, **179**, 529.
145 V. Dousset, C. Delalande, L. Ballarino, B. Quesson, D. Seilhan, M. Coussemacq, E. Thiaudiere, B. Brochet, P. Canioni and J. M. Caille, *Magn. Reson. Med.*, 1999, **41**, 329.
146 B. Arvin, L. F. Neville, F. C. Barone and G. Z. Feuerstein, *Neurosci Biobehav R*, 1996, **20**, 445.
147 W. Li, S. Tutton, A. T. Vu, L. Pierchala, B. S. Y. Li, J. M. Lewis, P. V. Prasad and R. R. Edelman, *J. Magn. Reson. Imaging*, 2005, **21**, 46.
148 P. Reimer, C. Marx, E. J. Rummeny, M. Muller, M. Lentschig, T. Balzer, K. H. Dietl, U. Sulkowski, T. Berns, K. Shamsi and P. E. Peters, *J. Magn. Reson. Imaging*, 1997, **7**, 945.

149 C. Klein, S. Schalla, B. Schnackenburg, A. Bornstedt, V. Hoffmann, E. Fleck and E. Nagel, *J. Magn. Reson. Imaging*, 2003, **17**, 656.
150 A. Schnorr, S. Wagner, C. Abramjuk, I. Wojner, T. Schink, T. J. Kroencke, E. Schellenberger, B. Hamm, H. Pilgrimm and M. Taupitz, *Invest. Radiol.*, 2004, **39**, 546.
151 A. E. Stillman, N. Wilke, D. B. Li, E. M. Haacke and S. McLachlan, *J. Comput. Assisted Tomogr.*, 1996, **20**, 51.
152 A. E. Stillman, N. Wilke and M. Jerosch-Herold, *J. Magn. Reson. Imaging*, 1997, **7**, 765.
153 W. W. Mayo-Smith, S. Saini, G. Slater, J. A. Kaufman, P. Sharma and P. F. Hahn, *Am. J. Roentgenol.*, 1996, **166**, 73.
154 L. Rohl, L. Ostergaard, C. Z. Simonsen, P. Vestergaard-Poulsen, L. Sorensen, A. Bjornerud, K. B. Saebo and C. Gyldensted, *Acta Radiologica*, 1999, **40**, 282.
155 A. M. Taylor, J. R. Panting, J. Keegan, P. D. Gatehouse, D. Amin, P. Jhooti, G. Z. Yang, S. McGill, E. D. Burman, J. M. Francis, D. N. Firmin and D. J. Pennell, *J. Magn. Reson. Imaging*, 1999, **9**, 220.
156 K. H. Ahlstrom, L. O. Johansson, J. B. Rodenburg, A. S. Ragnarsson, P. Akeson and A. Borseth, *Radiology*, 1999, **211**, 865.
157 D. Weishaupt, P. R. Hilfiker, M. Schmidt and J. F. Debatin, *Cardiovascular and Interventional Radiology*, 1999, **22**, 321.
158 P. R. Hilfiker, G. G. Zimmermann-Paul, M. Schmidt, H. P. Klotz, G. M. Kacl and J. F. Debatin, *Radiology*, 1998, **209**, 769.
159 T. Ichikawa, A. S. Arbab, T. Araki, K. Touyama, H. Haradome, J. Hachiya, M. Yamaguchi, H. Kumagai and S. Aoki, *Am. J. Roentgenol.*, 1999, **173**, 207.
160 H. E. Daldrup-Link, J. Rydland, T. H. Helbich, A. Bjornerud, K. Turetschek, K. A. Kvistad, E. Kaindl, T. M. Link, K. Staudacher, D. Shames, R. C. Brasch, O. Haraldseth and E. J. Rummeny, *Radiology*, 2003, **229**, 885.
161 M. Kresse, S. Wagner, D. Pfefferer, R. Lawaczeck, V. Elste and W. Semmler, *Magn. Reson. Med.*, 1998, **40**, 236.
162 T. Suwa, S. Ozawa, M. Ueda, N. Ando and M. Kitajima, *Int. J. Cancer*, 1998, **75**, 626.
163 L. G. Remsen, C. I. McCormick, S. RomanGoldstein, G. Nilaver, R. Weissleder, A. Bogdanov, K. E. Hellstrom, I. Hellstrom, R. A. Kroll and E. A. Neuwelt, *Am. J. Neuroradiol.*, 1996, **17**, 411.
164 R. Weissleder, A. S. Lee, A. J. Fischman, P. Reimer, T. Shen, R. Wilkinson, R. J. Callahan and T. J. Brady, *Radiology*, 1991, **181**, 245.
165 M. Zhao, M. F. Kircher, L. Josephson and R. Weissleder, *Bioconjugate Chem.*, 2002, **13**, 840.
166 L. Josephson, C. H. Tung, A. Moore and R. Weissleder, *Bioconjugate Chem.*, 1999, **10**, 186.
167 X. Montet, K. Montet-Abou, F. Reynolds, R. Weissleder and L. Josephson, *Neoplasia*, 2006, **8**, 214.
168 X. Montet, M. Funovics, K. Montet-Abou, R. Weissleder and L. Josephson, *J. Med. Chem.*, 2006, **49**, 6087.
169 C. F. Zhang, M. Jugold, E. C. Woenne, T. Lammers, B. Morgenstern, M. M. Mueller, H. Zentgraf, M. Bock, M. Eisenhut, W. Semmler and F. Kiessling, *Cancer Res.*, 2007, **67**, 1555.
170 C. Sun, O. Veiseh, J. Gunn, C. Fang, S. Hansen, D. Lee, R. Sze, R. G. Ellenbogen, J. Olson and M. Q. Zhang, *Small*, 2008, **4**, 372.
171 C. Sun, R. Sze and M. Q. Zhang, *J. Biomed. Mater. Res. Part A*, 2006, **78A**, 550.
172 T. J. Chen, T. H. Cheng, Y. C. Hung, K. T. Lin, G. C. Liu and Y. M. Wang, *J. Biomed. Mater. Res. Part A*, 2008, **87A**, 165.
173 M. F. Kircher, J. R. Allport, E. E. Graves, V. Love, L. Josephson, A. H. Lichtman and R. Weissleder, *Cancer Res.*, 2003, **63**, 6838.
174 J. R. McCarthy, K. A. Kelly, E. Y. Sun and R. Weissleder, *Nanomedicine*, 2007, **2**, 153.
175 S. Cerdan, H. R. Lotscher, B. Kunnecke and J. Seelig, *Magn. Reson. Med.*, 1989, **12**, 151.
176 R. K. Jain, *Cancer Res.*, 1987, **47**, 3039.
177 S. E. MNneil, *J. Leukocyte Biol.*, 2005, **78**, 585.
178 D. G. Stupack and D. A. Cheresh, in *Current Topics in Developmental Biology*, ed. G. P. Schatten, Elsevier, Amsterdam, 2004, vol. 64, pp. 207.
179 C. J. Sunderland, M. Steiert, J. E. Talmadge, A. M. Derfus and S. E. Barry, *Drug Dev. Res.*, 2006, **67**, 70.
180 S. D. Weitman, R. H. Lark, L. R. Coney, D. W. Fort, V. Frasca, V. R. Zurawski and B. A. Kamen, *Cancer Res.*, 1992, **52**, 3396.
181 J. F. Ross, P. K. Chaudhuri and M. Ratnam, *Cancer*, 1994, **73**, 2432.
182 H. Choi, S. R. Choi, R. Zhou, H. F. Kung and I. W. Chen, *Acad. Radiol.*, 2004, **11**, 996.
183 M. E. Dudley, J. R. Wunderlich, P. F. Robbins, J. C. Yang, P. Hwu, D. J. Schwartzentruber, S. L. Topalian, R. Sherry, N. P. Restifo, A. M. Hubicki, M. R. Robinson, M. Raffeld, P. Duray, C. A. Seipp, L. Rogers-Freezer, K. E. Morton, S. A. Mavroukakis, D. E. White and S. A. Rosenberg, *Science*, 2002, **298**, 850.
184 F. H. Valone, E. Small, M. MacKenzie, P. Burch, M. Lacy, M. V. Peshwa and R. Laus, *Cancer J.*, 2001, **7**, S53.
185 N. Bessis, V. Cottard, N. Saidenberg-Kermanach, D. Lemeiter, C. Fournier and M. C. Boissier, *J. Gene Med.*, 2002, **4**, 300.
186 H. T. Song, J. S. Choi, Y. M. Huh, S. Kim, Y. W. Jun, J. S. Suh and J. W. Cheon, *J. Am. Chem. Soc.*, 2005, **127**, 9992.
187 M. Lewin, N. Carlesso, C. H. Tung, X. W. Tang, D. Cory, D. T. Scadden and R. Weissleder, *Nat. Biotechnol.*, 2000, **18**, 410.
188 J. S. Choi, J. C. Park, H. Nah, S. Woo, J. Oh, K. M. Kim, G. J. Cheon, Y. Chang, J. Yoo and J. W. Cheon, *Angew. Chem. Int. Ed. Engl.*, 2008, **47**, 6259.
189 S. P. Manninger, L. L. Muldoon, G. Nesbit, T. Murillo, P. M. Jacobs and E. A. Neuwelt, *Am. J. Neuroradiol.*, 2005, **26**, 2290.